SAPIENZA
UNIVERSITÀ DI ROMA

Research Doctorate in:

Clinical/Experimental Neuroscience and Psychiatry

PhD Program:

Experimental Neurology

Title of the Thesis:

"*In vivo* analyses of the correlates of cortical and white matter pathology in patients with multiple sclerosis by quantitative 7 Tesla and 3 Tesla MRI and molecular imaging"

Mentor
Prof. Carlo Pozzilli

PhD Candidate
Dr. Valeria Barletta

Supervisor
Prof. Caterina Mainero

Academic year 2019/2020

Index

Preface

The data presented in this thesis have been produced during my research activity at Harvard Medical School, in the Multiple Sclerosis Laboratory located at Athinoula A. Martinos Center for Biomedical Imaging, Boston, under the supervision of Professor Caterina Mainero.

The two projects here reported were conducted during the period covering my entire PhD program, between 2017 and 2020. During these years I improved my expertise in the field of advanced neuroimaging applied to the study of multiple sclerosis pathology.

This research thesis is dedicated to all the people affected by multiple sclerosis.

Abstract

This thesis is divided in two sections. The first reports the results from a project regarding the application of ultra-high-field quantitative MRI for the study of cortical grey matter pathology in patients with early multiple sclerosis (MS). Applying a Combined Myelin Estimation method, obtained by 7 Tesla magnetic resonance imaging, we aimed at characterizing cortical microstructural abnormalities related to myelin content in cortical lesions and normal-appearing cortex, to assess their evolution at 1-year follow-up and to relate cortical myelin changes to clinical and radiological disease burden.

Data obtained from 25 patients with early MS and 19 healthy volunteers showed overall abnormally low myelin content in cortical lesions and several areas of normal-appearing cortex. Myelin content along the cortex correlated with neurological impairment. Individual cortical lesion analysis revealed heterogenous patterns, ranging from extensive to partial demyelination, or even measurements comparable to the healthy group. At 1-year follow-up, cortical myelin was overall decreased in cortical lesions and scattered areas in the normal-appearing cortex. Diffusion metrics obtained in the same regions did not show the presence of cortical neural loss accompanying early demyelination.

The second section reports results from a study in which we combined ^{11}C-PBR28 positron-emission tomography, marking activated microglia, with the more recently validated synthetic magnetic resonance imaging for myelin content assessment, aiming at researching the presence of correlates of pathology in the white matter of patients with multiple sclerosis at different disease stages, and assessing the interplay between neuroinflammation and demyelination. We found abnormal increase of microglia activation in MS patients compared to healthy volunteers in several areas across the white matter, correlating with clinical and radiological disease burden. An individual analysis of white matter lesions showed the presence of active lesions in the early phases of the disease, evolving in inactive or peripherally active lesions in the late disease phases, the latter correlating with clinical disability. Myelin content in the normal-appearing white matter of MS patients correlated with neurological impairment and lesion load. Higher microglia activation in the white matter lesions was related to lower myelin content in the non-lesioned white matter.

Section 1

Quantitative 7-Tesla imaging of cortical microstructural changes in patients with early multiple sclerosis

Summary

Objectives. To characterize cortical microstructural abnormalities related to myelin content in early multiple sclerosis by a quantitative Combined Myelin Estimation (CME) method obtained by 7 Tesla magnetic resonance imaging (MRI); to assess the evolution of cortical abnormalities at 1-year follow-up; to relate cortical myelin content to clinical and radiological disease burden.

Methods. We prospectively enrolled 25 patients with early multiple sclerosis and 19 age-matched healthy volunteers. Ten MS patients were re-scanned after one year. A cortical CME map was obtained from quantitative 7-Tesla T2* and T1 acquisitions.

At baseline, patients' cortical lesions were classified based on their myelin content by comparison with mean CME values of the control group in corresponding cortical regions. To account for other factors influencing myelin estimation, including neurite/dendrite loss, cortical measurements from the neurite orientation dispersion and density imaging diffusion model were assessed. CME was correlated to clinical and radiological metrics. Cortical CME abnormalities were also investigated vertex-wise at baseline and 1-year follow-up.

For validation, cortical CME in healthy volunteers was correlated to myelin optical measurements from histology.

Results. In patients, CME was overall abnormally low in cortical lesions and several areas of normal-appearing cortex, as indicated by voxel-wise analysis. CME values along the cortex correlated with neurological impairment. Individual cortical lesion analysis revealed, heterogenous CME patterns ranging from extensive to partial demyelination (60% of lesions), or values comparable to the healthy group.

In healthy volunteers, cortical CME correlated with histological optical myelin measures from the healthy cortex, thus providing validation of the technique.

At 1-year follow-up, CME was overall decreased in cortical lesions and scattered areas in the normal-appearing cortex. Diffusion metrics did not show cortical neural loss, but higher orientation dispersion accompanied an increase of CME at follow-up.

Conclusion. Heterogeneous cortical microstructural changes, likely due to coexisting demyelination, incomplete demyelination and remyelination, can be imagined *in vivo* in early multiple sclerosis. The correlation between cortical myelin content and EDSS is ambivalent, possibly due to low disability in the early disease phase. A positive correlation was found between cortical myelin content and processing speed. Demyelination was not accompanied by neural loss, as detected by diffusion imaging, but a higher dendrite arborization was found in remyelinating lesions.

Introduction

1.1 Cortical lesions in multiple sclerosis

Cortical demyelinating lesions are a pathologic hallmark of multiple sclerosis (MS) and can develop from the early stages of the disease (Calabrese et al., 2007). They relate to clinical disability and disease progression (Peterson et al., 2001; Lucchinetti et al., 2011; Calabrese et al., 2010; Mainero et al., 2015; Treaba et al., 2019).

Demyelination in the cortex mainly affects the subpial layers and is associated with inflammatory infiltrates in the meninges (Kutzelnigg et al., 2005; Lucchinetti et al., 2011). Based on the presence of myelin degradation products inside macrophages and microglia, cortical lesions can be distinguished in actively demyelinating or post-demyelinating (Lucchinetti et al., 2011; Kuhlmann et al., 2017). Moreover, ongoing demyelination can coexist with massive remyelination within the same lesion (Prineas et al., 1984). The efficiency of remyelination in the brain in MS seems to change according to disease type and anatomical location (Patrikios et al., 2006; Albert et al., 2007).

In the cortex, remyelination has been suggested to occur to a wider extent than in white matter, possibly due to higher availability of oligodendrocytes and their precursors (Albert et al., 2007, Strijbis et al., 2017). Cortical remyelination in MS patients shows a heterogeneous pattern within lesions. In an ex vivo study of chronic MS, extensive remyelination was present in 18% of cortical lesions, while most lesions showed remyelination restricted to the lesion border (Albert et al., 2007). Pathology studies, however, are skewed towards cases with late disease stage, often with associated comorbidities.

Experimental models of MS provide ample evidence of remyelination, both in cell cultures and animals (van der Star et al., 2012; Lassmann et al., 2017). Compared to ex vivo examinations, experimental studies allow testing for effective treatments in addition to providing a deep understanding of the biological phenomena related to remyelination. However, the biological differences between the system in which demyelination is induced (cell cultures, animals) and the artificial induction of demyelination itself (viral infection, chemical, immunological) make these models only partially comparable to the human disease.

The extent and clinical impact of cortical demyelination and concomitant remyelination in MS patients are still unclear. It is not known whether some patients show better propensity

for endogenous remyelination than others. Neither is known whether the presence or absence of remyelination in these patients might have an influence on the disease course.

In vivo studies are, thus, needed to increase our knowledge on the presence, extent and clinical impact of remyelination in MS. In white matter lesions (WML), initial data using 11C-PiB PET demonstrate dynamic remyelination in active relapsing-remitting MS (RRMS) patients, which can be detected as early as 2-4 months following the baseline evaluation (Bodini et al., 2016).

1.2 *In vivo* characterization of cortical pathology in multiple sclerosis

In vivo imaging of cortical lesions with MRI in MS, especially the subpial type, is still suboptimal. The geometry of the cortex and the small dimensions of cortical plaques represent an important technical challenge in the development of imaging tools for detecting and monitoring cortical lesion demyelination and remyelination.

Ultra-high field 7 Tesla (7T) MRI more than doubles detection of cortical MS lesions compared to lower field strengths. The sensitivity at 7T seems to depend on cortical lesion type, with T2* providing a relative benefit relative to other contrasts in visualizing intracortical lesions (Pitt et al., 2010; Kilsdonk et al., 2016). Analyses of cortical myelin integrity on a voxel- or vertex-wise basis can also overcome some of the limitations and biases that arise from detection of cortical lesions based on visual inspection of scans (Cohen-Adad et al., 2011). A series of "semi-quantitative" (magnetization transfer ratio imaging, diffusion imaging, T2/T1-weighted), and "quantitative" (T2, T2*, T1) MRI approaches have been used in MS (Derakhshan et al., 2014; Mainero et al., 2015; Guglielmetti et al., 2016). None of them, however, is exclusively specific for myelin, as each can be affected by sequence parameters and biological components of the cortex (water content, iron, cells, fiber density).

Surface-based estimation of ultra-high resolution quantitative T2* at 7T in vivo is highly reproducible (Govindarajan et al., 2015) and can reveal the myelo-architecture organization of the human cortex, as well as microstructural intracortical changes in MS as a function of cortical depth, likely related to demyelination (Cohen-Adad et al., 2012; Mainero et al., 2015). However, as myelin fibers co-localize with iron in both the white matter and the cortex, T2* is affected by the presence of iron, with ferritin iron content representing the primary source of the intracortical T2* contrast (Fukunaga et al., 2010).

1.3 The Combined Myelin Estimation model

In a previous study we developed a multivariate model for extracting 7T quantitative T2* and 3T magnetization transfer ratio shared information to obtain the Combined Myelin Estimation (CME), an index sensitive to cortical myelin content in healthy subjects, limiting confounding factors including iron, cortical thickness (related to partial volume effect) and B0 inhomogeneity. Results of the CME spatial distribution obtained with this model showed similar trends to that from histological work stained for myelin (Mangeat et al., 2015). More recently, we applied the CME model in healthy volunteers and patients with MS to integrate myelin-related information from quantitative T2* and T1 maps from 7T acquisitions and demonstrated excellent reproducibility of the technique and better specificity to MS pathology compared to T2* and T1 metrics alone (Mangeat et al., 2018). Longitudinal relaxation time T1 correlates with brain myelin content (Koenig et al., 1990; Stüber et al., 2014) but is less influenced by the presence of iron than T2* (Stüber et al., 2014). T1, however, also correlates with cortical neuronal content in MS brain samples (Schmierer et al., 2010).

1.4 The Neurite Orientation Dispersion and Density Imaging model

The Neurite Orientation Dispersion and Density Imaging (NODDI) is a multicompartment diffusion MRI model that showed high specificity in providing microstructural neuronal indices in vivo (Zhang et al. 2012; Grussu et al. 2017). The parameters obtained from this model are the neurite density index (NDI), the orientation dispersion index (ODI) and the isotropic volume fraction (IVF). The latter shows the signal contribution of the free isotropic Gaussian diffusion of cerebrospinal fluid or edema.

The NDI is a measure of neurite density, but also proved to correlate with myelin in the healthy brain and in MS (Jespersen et al., 2010; Zhang et al., 2012; Grussu et al., 2017). In the healthy brain, this parameter is higher in the white matter, reflecting the density of myelinated axons, and lower in the grey matter (Jespersen et al. 2010). *In vivo* and *ex vivo* studies on MS showed a decrease of NDI in white matter and cortical lesions and in the normal-appearing white matter (Granberg et al. 2017; Grussu et al., 2017; Schneider et al., 2017; Collorone et al., 2020).

The ODI is a measure of neurite dispersion. Its values are lower in the white matter, were neurites are tightly organized, and higher in the grey matter because of dendrite arborization, thus providing an index of grey matter complexity (Zhang et al., 2012). However, its measurements in MS studies seem to give discordant results, also based on the magnetic field

strength at which the parameter was obtained (Granberg et al., 2017; Grussu et al., 2017; Schneider et al., 2017; De Santis et al., 2019).

1.5 Hypotheses and aims

We hypothesized that cortical microstructural alterations, likely related to myelin content abnormalities, could be measured *in vivo* using the CME obtained from 7T quantitative T2* and T1 mapping in a cohort of 25 early MS cases relative to 19 age-matched healthy volunteers in both lesioned and normal-appearing cortex, and would evolve dynamically in time, suggesting cortical demyelination and remyelination phenomena. As myelin content could be influenced by additional pathological factors including neurite/dendrite loss, measurements from the diffusion model were obtained along CME in cortical lesions and whole cortex.

Secondarily, the relevance of cortical CME abnormalities on clinical and radiological estimates of disease burden was investigated.

Finally, to further validate the CME technique, we assessed the relation between cortical CME values in the healthy cohort and *ex vivo* myelin density optical measurements previously obtained across several Brodmann areas.

Methods

1.6 Subjects and clinical assessments

The Institutional Review Board approved this prospective cohort study protocol, and subjects gave written informed consent to participate in the study according to the Declaration of Helsinki.

General inclusion criteria were: age 18-60 years, no significant medical history (other than MS for patients), and absence of MRI contraindications. Eligibility criteria for MS subjects were: diagnosis RRMS diagnosis according to the McDonald criteria (Polman et al., 2011), disease duration ≤5 years, stable disease-modifying treatment or no treatment for at least 3 months, no relapses in the 3 months prior to enrolment, no corticosteroids use for at least 1 month prior to enrolment.

Twenty-five early MS patients (mean age 38.2±8.9; females: 21) with disease duration ≤5 years and 19 healthy controls (mean age 35.8±10.2; females: 10) were prospectively enrolled in the study.

All MS patients underwent a neurological examination with assessment of Expanded Disability Status Scale (EDSS) score and Symbol Digit Modalities Test (SDMT). One patient could not perform SDMT because of severe visual impairment. SDMT raw scores were converted to Z-scores (SDMTz) after correcting for age and years of education (Parmenter et al., 2010).

1.7 MRI acquisition protocol

All subjects were scanned on a 7T MRI whole-body scanner (MAGNETOM Siemens Healthcare) equipped with a 32-channel receive head coil, and on a 3T whole-body MRI scanner (MAGNETOM Skyra CONNECTOM, Siemens Healthcare), using a 64-channel head coil, within one week from the 7T scan. Ten MS patients were re-scanned with the same protocols at 1-year follow-up (mean follow-up time 1.0±0.2 years).

The 7T protocol included: two-dimensional fast low-angle shot T2*-weighted spoiled gradient-echo (GRE) images (0.33 x 0.33 x 1 mm, repetition time/echo time [TR/TE] = 1700/21.8 ms) for lesion segmentation; 2D GRE sequence (0.5 mm isotropic, TR=3680 ms, TE=3.12+3.32*[1..6] ms, 6 echoes, TA=40 min) to compute T2* maps; 3D dual magnetization-prepared rapid GRE sequence (MP2RAGE, 0.75 mm isotropic,

TR/TE/TI=5000/2.93/[900–3200] ms, flip angles=4° and 5°, TA=10 min) to compute T1 maps.

At 3T, we acquired a 3D T1-weighted image multi-echo magnetization prepared rapid acquisition GRE (MPRAGE, 1 mm isotropic, TR=2530, TE=[1.15, 3.03, 4.89, 6.75] ms, TI=1100 ms) for cortical surface reconstruction (Van der Kouwe et al., 2008). Multi-shell diffusion-weighted images were acquired using a 2D echo-planar imaging sequence (1.5 mm isotropic, b-values 1000 and 5000 s/mm2 with 64 and 128 diffusion weighting directions).

Figure 1.1 summarized the imaging study procedures.

1.8 Quantitative MRI analysis

Surface-based analysis—The cortical surface of each subject was extracted using FreeSurfer 5.3.0 (http://freesurfer.net) from the 3T MPRAGE after correction for gradient non-linearity-induced distortions. We used the 3T rather than the 7T images because the 7T scanner produced more B1+ inhomogeneities, potentially yielding more errors in the segmentations. Each surface reconstruction was carefully inspected any topographical errors caused by lesions were semi-manually corrected with lesion in-painting. The 7T quantitative T1 and T2* volumes were also corrected for gradient non-linearity distortions and then registered to the subject's surface using rigid (6 degrees of freedom, DOF) and affine (12 DOF) surface registration methods. Finally, T1 and T2* volumes were sampled at mid-cortical depth along the cortex and projected to the FreeSurfer average (fsaverage) space. Cortical thickness was computed to correct both metrics for partial volume effects on a per-vertex level.

Combination of 7T quantitative maps—A spatial independent component analysis was applied to the data to extract the myelin-specific signal shared by both metrics. This procedure produces a composite map, the CME map, that contains the myelin information from both the T2* and T1 maps (figure 1.1). The CME map has been suggested to be more specific to myelin content than the T2* and T1 maps separately (Badji et al., 2016; Mangeat et al., 2016, 2015b).

1.9 Diffusion modeling

Diffusion-weighted images were corrected for gradient non-linearities, eddy-current distortions and for subject motion using interspersed non-diffusion weighted images (Fan et al. 2016). After preprocessing, the two-shell high-angular resolution diffusion-weighted volumes were analyzed using the NODDI toolbox (v. 0.9, University College London,

London, UK, http://mig.cs.ucl.ac.uk/mig/mig/index.php/?n=Tutorial.NODDImatlab/) (Zhang et al., 2012).

Individual maps of diffusion-based metrics (ODI and NDI) were registered via their corresponding non-diffusion weighted echo-planar images to the cortical FreeSurfer reconstructions using a boundary-based registration with 12 degrees of freedom (Greve and Fischl 2009). To minimize partial volume effects, NODDI metrics were sampled across the whole cortex at mid-cortical depth (Granberg et al. 2017) (figure 1.1).

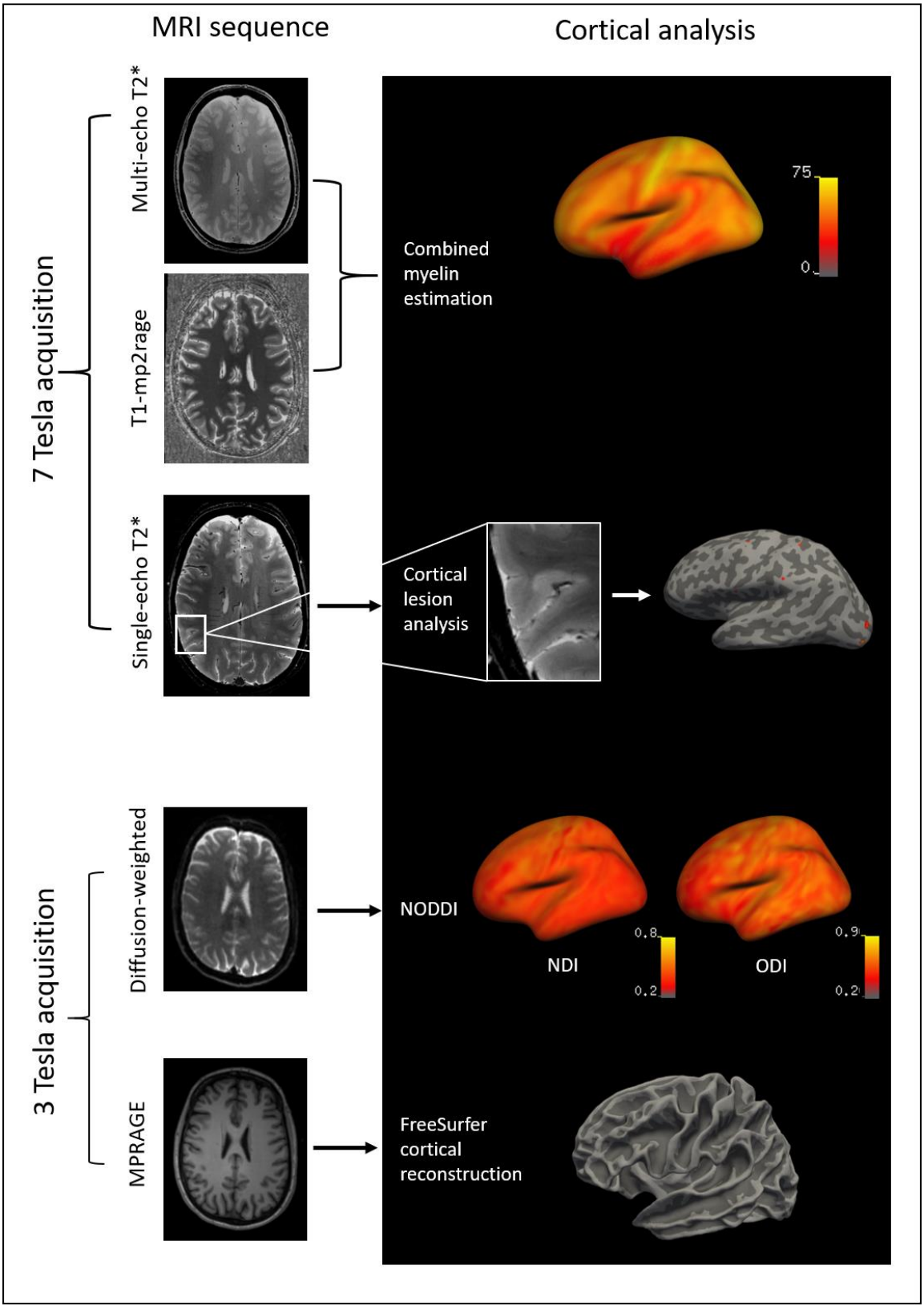

Figure 1.2. Methodology of the imaging analysis: 7 Tesla Multi-echo T1-mp2rage and T2* sequences were combined by independent component analysis to obtain cortical CME maps. Cortical lesions were segmented on 7Tesla single-echo T* star sequences and projected to the subject's surface. Diffusion-weighted images at 3 Tesla (b-values=1000 and 5000 s/mm^2; diffusion directions=64 and 128) were acquired to obtain cortical NODDI maps. T1-weighted

MPRAGE images at 3 Tesla were acquired for FreeSurfer cortical reconstructions. CME=combined myelin estimation. Mp2rage = dual magnetization-prepared rapid gradient echo. MPRAGE=magnetization prepared rapid acquisition gradient echo. NODDI= neurite orientation dispersion and density imaging. NDI=neurite density index. ODI=orientation dispersion index.

1.10 Lesion quantification and analysis

Intracortical, leukocortical and white matter lesions were manually segmented on Slicer (version 4.4.0, 2014, http://www.slicer.org) on T2*-weighted single echo images and checked on the corresponding T1 maps from 7T MP2RAGE acquisitions by active collaboration of one radiologist and one neurologist (figure 1.2). New lesions were identified on a lesion-by-lesion basis through agreement. Lesions were identified as focal hyperintensities that extended for at least 3 voxels and across 2 consecutive slices (Louapre et al., 2015). Lesion volumes were quantified by FSL using fslstats from FMRIB Software Library, v. 5.0 (http://fsl.fmrib.ox.ac.uk/fsl). Masks of normal-appearing cortex were obtained by subtracting the lesion masks from the whole cortex by using *fslmaths* on FSL.

Values for CME and NODDI were extracted at 50% cortical depth in cortical lesion masks and normal-appearing cortex. Since the focus of the study was the cortex, CME and NODDI for leukocortical lesions were measured only in the intracortical portion of the mask.

At baseline, myelination status for each cortical lesion was defined based on the percentage of voxels that had CME values ≤2 SD of the mean CME value in the corresponding cortical area in the control group using the Desikan-Killiany atlas in FreeSurfer. This was done to account for differences in myelo-architecture across the cortex. Based on the percentage of voxels with reduced CME within an individual lesion, cortical lesions were then classified as demyelinated (≥50%), partially demyelinated (5-49%), non-demyelinated (<5%). At follow up, we registered significant changes in CME (increased, decreased or stable) within each individual lesion as a variation of at least 1 SD from the basal value (Bodini et al., 2016).

Figure 1.2. White matter (green), leuko-cortical (yellow) and intracortical (red) lesion segmentation on 7 Tesla single-echo T2* sequences.

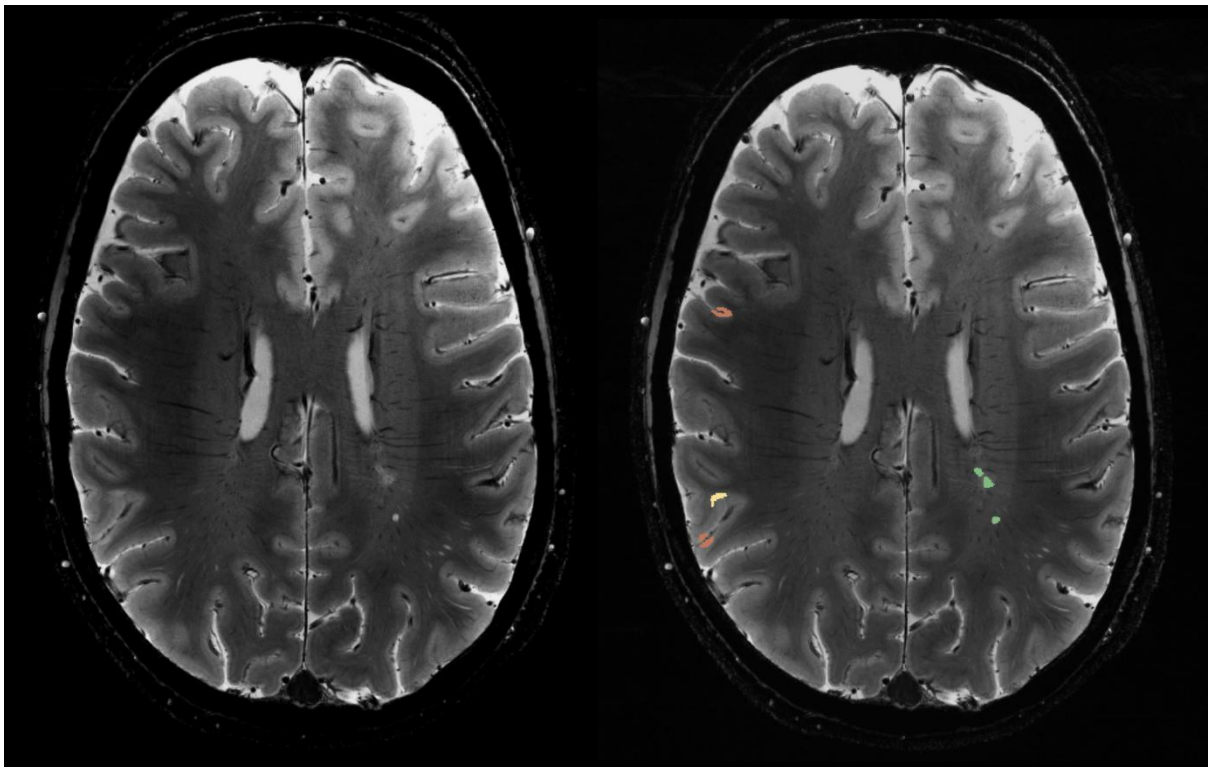

1.11 Surface-based group analyses of CME and NODDI

Individual surfaces of CME and NODDI metrics were registered to a common template surface in FreeSurfer and smoothed with a fullwidth at half-maximum kernel of 5 and 10 mm respectively. For CME, a general linear model (GLM) was used vertex-wise across the normal-appearing cortex, at three cortical depths, to i) correlate in control subjects CME with myelin measurements from histology ii) assess differences between patients and controls, iii) assess longitudinal CME changes in patients, iv) correlate cortical CME to EDSS and SDMT-z.

Vertex-wise GLM analysis was used to investigate differences in NDI and ODI between patients and healthy controls across the cortex. In all GLM analyses, a cluster-wise correction for multiple comparisons using Monte Carlo simulation with 10,000 iterations was applied. Significant clusters were localized using the Desikan-Killiany atlas in FreeSurfer.

1.12 Statistical analysis

Statistical was performed on JMP pro v13. A p-value <0.05 was considered significant.

Demographics were compared between patients and controls by Wilcoxon test. Multilinear regression with age and gender as nuisance factor was used to compare cortical thickness in patients versus healthy volunteers. Pearson correlation was used to compare CME in healthy controls and myelin measurements from histology (Braitenberg 1962; Mangeat et al., 2015).

Matched paired-t test was used to assess i) CME and NODDI in cortical lesions versus normal-appearing homologous contralateral grey matter, ii) cortical lesion CME and NODDI changes at follow-up, iii) changes in cortical lesion and white matter lesion volume at follow-up. A multilinear regression, including age as a nuisance factor, was used to compare CME in cortical lesions versus cortical grey matter in healthy controls.

Nominal logistic regression was used to correlate CME status at baseline (demyelinated, partially demyelinated, non-demyelinated) to NODDI continuous values and to correlate CME status at follow-up (increased, decreased, stable) to lesion type. Subject ID was included in the analysis as a confounding factor. Multilinear regression was applied to compare NODDI at baseline and follow-up in individual lesions divided based on CME status at follow-up. Subjects ID was a confounding factor.

Repeated measures correlation, to account for different cortical lesion count among subjects, was applied to check for correlations between CME in cortical lesions and clinical and MRI parameters. MRI parameters included in the analysis were cortical lesion count and volume, white matter lesion volume, cortical thickness. Clinical metrics included in the analysis were: disease duration, age at disease onset, EDSS, SDMT-z. Pearson's correlation related cortical thickness to EDSS and SDMT-z.

Results

1.13 Demographic, clinical and MRI results

The demographic, clinical and MRI characteristics of the study subjects are summarized in table 1.1. Twenty-five early MS patients (mean age 38.2±8.9; females: 21) with disease duration ≤5 years and 19 healthy controls (mean age 35.8±10.2; females: 10) were prospectively enrolled in the study. Ten MS patients (mean age 36±7.6 years; females: 8) were re-scanned after one-year (mean follow-up time 1.0±0.2 years).

At baseline, 103 cortical lesions were detected in 20/25 (80%) MS patients, 62 (60%) intracortical, 41 (40%) leukocortical (table 1.1). No lesions were detected in the healthy group.

At 1-year follow-up, 25 new cortical lesions (23 intracortical and 2 leukocortical) developed in 4/10 patients. Overall, both cortical and white matter lesion volumes tended to be higher at follow-up, although not significantly. Cortical thickness did not change significantly (table 1.2).

Diffusion NODDI images were acquired at baseline in 21 MS patients (18 of which showed cortical lesions) and 17 healthy controls, and in 9/10 patients re-scanned at 1-year follow-up.

Table 1.1. Demographic, clinical and radiological characteristics of the study subjects.

Characteristic	Healthy controls n = 19	MS patients n = 25	*P* value
Age, mean±SD	35.8±10.2	38.2±8.9	0.3*
Females number	10	21	0.04**
Disease duration in years, median (range)	-	1.9 (0.6-4.7)	-
Age at disease onset, mean±SD	-	35±8.1	-
EDSS, median (range)	-	2 (0-5)	-
SDMT z-score, median (range)	-	0.75 (-1.92, 3.3)	-
Disease modifying treatment n	-	22	-
- Dimethyl fumarate n	-	10	-
- Glatiramer acetate n	-	5	-
- Interferon beta-1a n	-	4	-
- Natalizumab n	-	2	-
- Ocrelizumab n	-	1	-
Cortical thickness in mm, mean±SD	2.43±0.1	2.40±0.1	0.89***
Total cortical lesion count, median (range)	-	2 (1-22)	-
Total cortical lesion volume mm^3, mean±SD	-	245±245	-
Intracortical lesion volume mm^3, mean±SD	-	162±161	-
Leukocortical lesion volume mm^3, mean±SD	-	164±180	-
White matter lesion volume mm^3, mean±SD	-	1357±2160	-

Note: MS=multiple sclerosis; SD=standard deviation; EDSS=expanded disability status scale; SDMT=symbol digit modalities test. *by Wilcoxon test; **by Fisher's exact test. *** by multilinear regression correcting for age and gender.

Table 1.2. MRI characteristics of the MS patients re-scanned after 1 year.

MRI characteristic	Baseline	follow-up	*P* value
Cortical thickness mm, mean±SD	2.40±0.08	2.41±0.07	0.67*
Total cortical lesion count, median (range)	5 (1-22)	5.5 (1-33)	-
White matter lesion volume mm^3, mean±SD	1350±2162	1472±2025	0.3*
Total cortical lesion volume mm^3, mean±SD	253±242	369±566	0.4*

Note: MS=multiple sclerosis. SD=standard deviation. *By matched pairs t test.

1.14 CME and NODDI metrics along the normal-appearing cortex

In healthy subjects, we found a positive correlation between CME at each cortical depth and myelin density optical measurements previously obtained in the corresponding cortical regions of a healthy adult human brain (Braitenberg 1962; Mangeat et al., 2015) (figure 1.3).

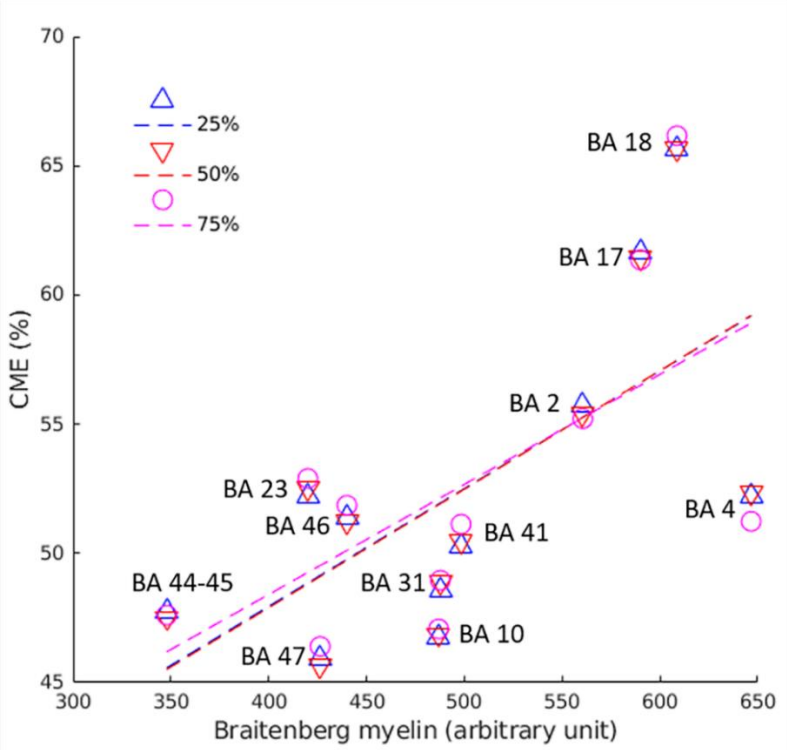

Figure 1.3. Pearson correlation between combined myelin estimation (CME) values in the healthy controls' cortex and Braitenberg's myelin optic measurements23 across 12 Brodmann areas (BA). Pearson coefficient was 0.6 (p=0.036) at 25%, 0.7 (p=0.022) at 50% and 0.7 (p=0.024) at 75% of cortical depth from the pial surface.

At baseline, the GLM analysis revealed several clusters of significantly reduced CME in MS patients compared to control group in the normal-appearing cortex at all cortical depths, especially in the precentral and postcentral gyri and in the supramarginal cortex, together with fewer areas in which CME was increased (figure 1.4 A). Supplemental table 1 summarizes the localization of the clusters in which CME values were significantly different in MS patients versus controls. No differences in NDI or ODI were seen at GLM analysis between patients and controls along the whole cortex.

In 10 patients re-scanned at 1-year follow-up, CME % was overall reduced in normal-appearing cortex (50.0±2 versus 49.7±2, p=0.02 by matched pairs t test). The GLM comparing vertex-wise CME sampled along the cortex at 25%, 50% and 75% depth showed areas of reduced CME at follow up relative to baseline along with fewer clusters with increased CME (figure 1.4 B).

Figure 1.4. Overlay of the general linear model significance maps ($p < 0.05$ corrected for multiple comparisons). A) Clusters of significantly reduced (blue) or increased (yellow) combined myelin estimation (CME) values in the normal appearing cortex of 25 patients with early multiple sclerosis versus 19 age-matched healthy controls. B) Variation in CME values in the normal appearing cortex of 10 MS patients re-scanned at one-year follow-up. Blue clusters indicate areas of CME reduction, yellow clusters indicate CME increase. Both analyses were performed on normal appearing cortex at three cortical depths (25%, 50%, 75%) from the pial surface, overlapped in the figure. Color bars show -log10(p value).

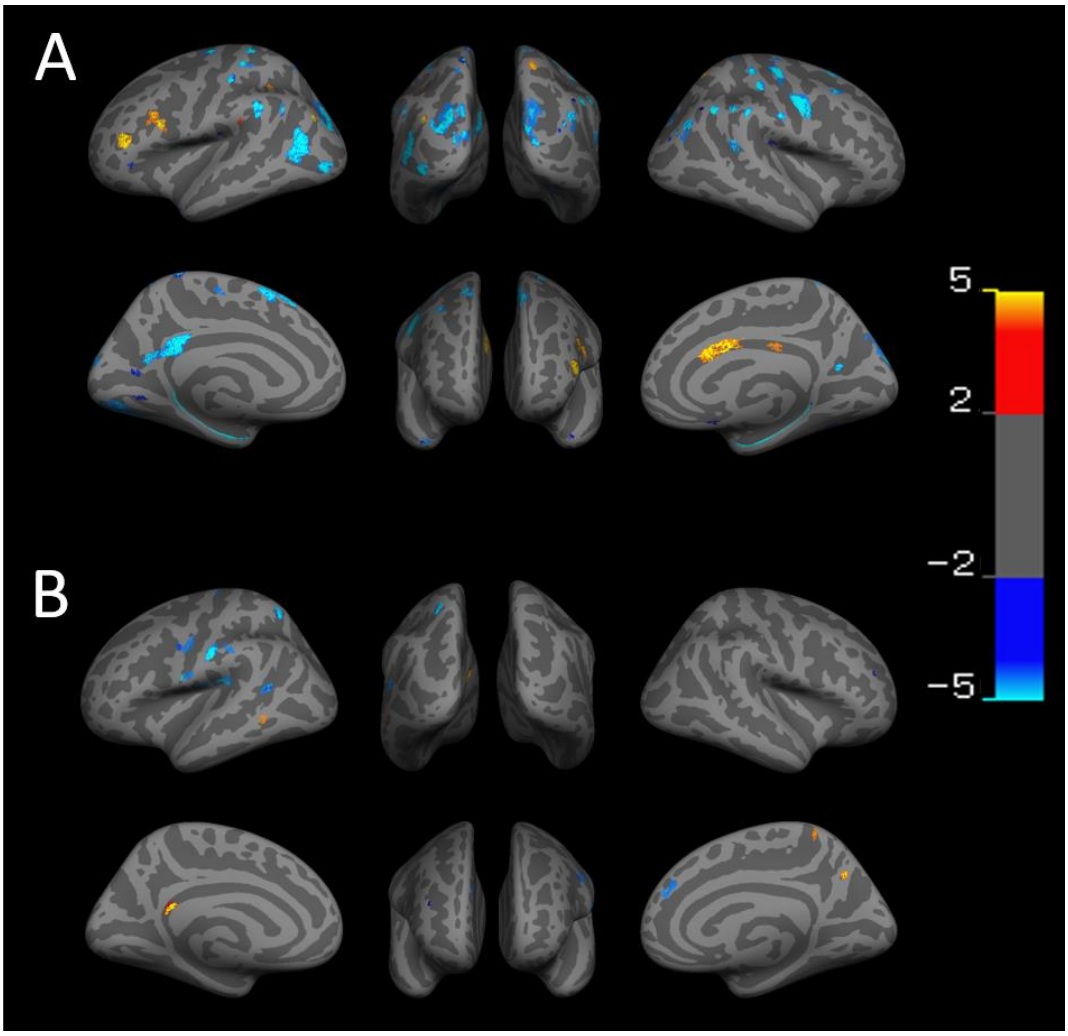

1.15 CME and NODDI metrics in cortical lesions

Overall, cortical lesions showed lower mean CME values relative to the contralateral normal-appearing cortex (p=0.04 by t test) and to healthy subjects' cortex (p=0.03 by multilinear regression), while no differences were detected for either NDI or ODI in the same regions (table 3).

Individual cortical lesion analysis showed that 62/103 (60%) of them were demyelinated, either extensively 33/103 (32%) or partially 29/103 (28%). The percentage of demyelination did not relate to lesion type (p=0.4 by Wilcoxon test for intracortical versus leukocortical). Forty-one out of 103 lesions showed <5% demyelinated voxels.

Values of NDI and ODI were extracted individually for 97 cortical lesions (18 MS subjects) at baseline. No difference was seen in either NDI or ODI in MS cortical lesions relative to the contralateral normal-appearing cortex in patients (respectively, p=0.4 and 0.6, by t test) and to the healthy controls' cortex (p=0.3 and 0.2 by multilinear regression) (table 1.3). Values of NDI and ODI were also grouped based on cortical lesion myelination status as measured by CME, and did not show any difference between demyelinated, partially demyelinated or non-demyelinated cortical plaques (for NDI p=0.6; for ODI p=0.7, by nominal logistic regression, subject ID was an adjusting factor).

At follow-up, cortical lesions showed an overall reduction in CME % (48.8±7.2 versus 46.5±6.1, p=0.03 by t test), suggesting further global demyelination.

Individual CME lesion analysis revealed that out of the total 63 lesions re-examined at follow-up, 26 (41%) showed reduction of their basal CME values >1 SD, 27 (43%) showed no significant changes, while 10 (16%) registered an increase ≥1 SD of CME basal values. Interestingly, two of the lesions with increased CME were fully demyelinated at baseline but reached mean CME values in the range of normality at follow-up, suggesting effective remyelination.

Lesion type (intracortical or leukocortical) was not a predictor of CME changes at follow up (p = 0.59 by nominal logistic regression).

No significant changes were seen in NODDI metrics in cortical lesions (by paired t test) at follow-up. However, when individual cortical lesions were divided based on CME changes at follow-up (increased, stable, decreased), a significant increase was seen in ODI in lesions with increased CME (ODI mean±SD 0.49±0.08 at baseline versus 0.57±0.02 at follow-up, p=0.009 by multilinear regression, subject ID was included as a confounding factor).

Table 1.3. Results from the Combined Myelin Estimation and Neurite Orientation Dispersion and Density Index modelling in the cortex of early stage multiple sclerosis subjects and healthy controls.

Metric	MS cortical lesions	MS contralateral normal appearing cortex	*P* value	MS whole cortex	Healthy controls whole cortex	*P* value
CME % mean±SD	47.1±6.4	50.0±8.6	0.04*	50.2±1.8	50.6±1.8	0.4**
NDI mean±SD	0.42±0.03	0.42±0.03	0.4*	0.43±0.01	0.43±0.02	0.8**
ODI mean±SD	0.55±0.04	0.56±0.05	0.6*	0.56±0.01	0.56±0.01	1.0**

MS=multiple sclerosis. CME=combined myelin estimation. NDI=neurite density index. ODI=orientation dispersion index. * by matched pairs t test. ** by multilinear regression (adjusted for age).

1.16 Correlations between CME and MRI and clinical disease burden

The repeated measures correlation analysis did not show any association between mean cortical lesion count and volume and white matter lesion load with clinical outcome metrics. No association was found between cortical thickness and either EDSS or SDMTz by Pearson correlation.

The GLM along the whole cortex showed significant clusters of correlations between CME sampled at three cortical depths and both EDSS and SDMTz (figure 1.5).

For EDSS, both positive and negative areas of correlation were found at the three depths, with positive clusters more represented at 25% from pial surface, and negative ones at 75% from pial surface. Negative clusters were mainly located in the precentral gyrus and inferior parietal cortex, positive clusters in the postcentral gyrus and the cingulate cortex (figure 1.5 A, table 1.4).

For SDMTz, we found that in the majority of cases, especially for clusters located at mid-cortical level, lower CME values correlated with lower SDMTz scores (figure 1.5 B). These clusters were mainly located in the left superior parietal, right inferior parietal and lateral occipital cortex, and in the right supramarginal gyrus (table 1.4).

Interestingly, an area located in the caudal anterior cingulate, where myelin content appeared to be increased in patients compared to healthy subjects, showed positive correlation with EDSS and negative with SDMTz (figure 1.5 C).

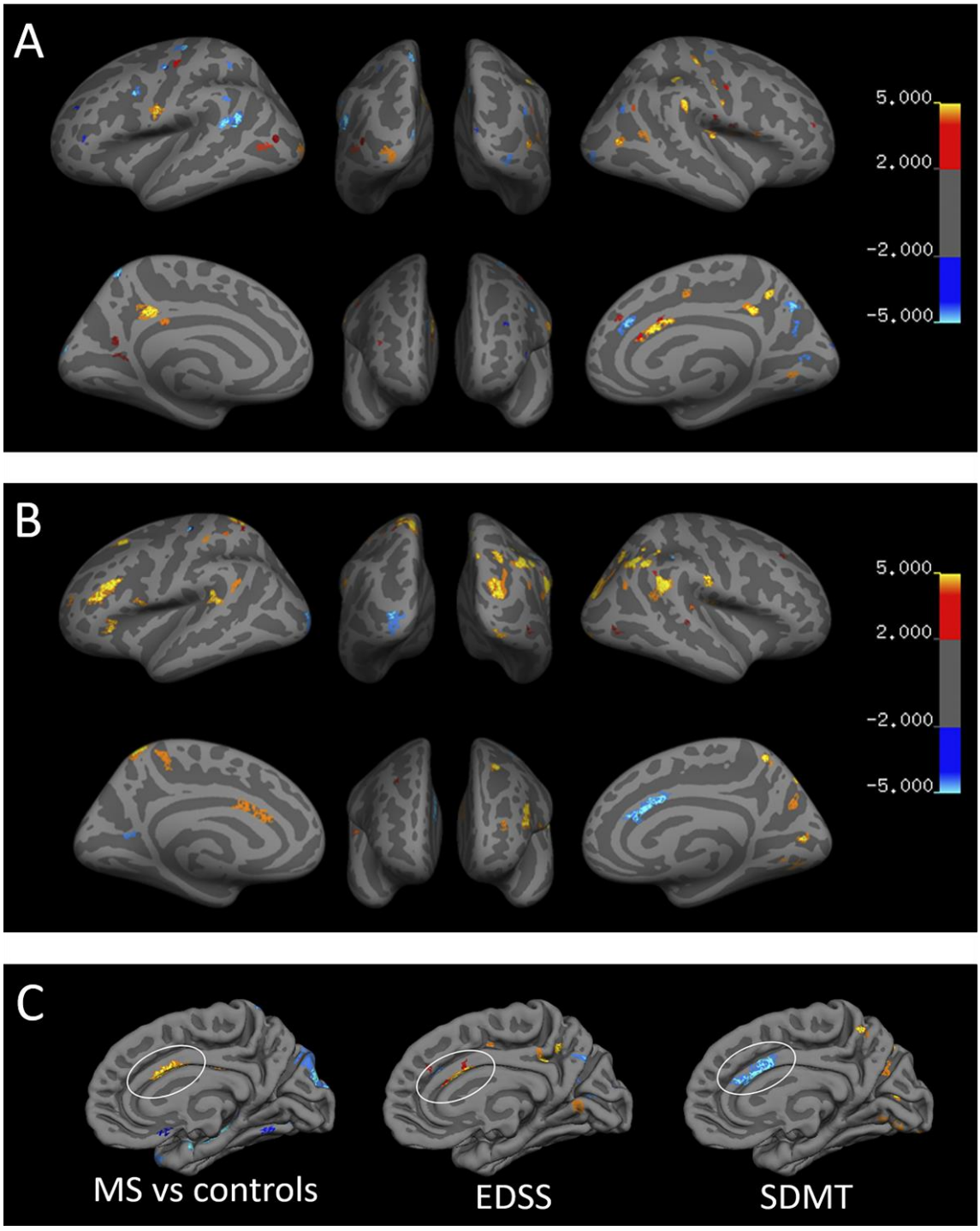

Figure 1.5. Overlay of the general linear model significance maps ($p < 0.05$ corrected for multiple comparisons) showing clusters of positive (blue) and negative (yellow/red) correlations between combined myelin estimation and (A); Expanded Disability Status Scale; (B) Symbol Digit Modalities Test Z-scores. Both analyses were performed at three cortical depths (25%, 50% and 75%) from the pial surface, overlapped in the figure. Color bars show -$\log_{10}$(p value). In (C), circled in white, cortical area in the right caudal anterior cingulate in which CME was significantly higher in MS patients than in healthy controls. In patients, this area showed positive correlation with EDSS scores and negative correlation with SDMT z scores.

Table 1.4. Localization of clusters indicating positive and negative correlations between Combined Myelin Estimation at three cortical depths and i) Expanded Disability Status Scales score ii) Symbol Digit Modalities Test Z-scores. The number of clusters is indicated in round brackets.

EDSS		
Negative correlation		
Cortical depth - distance from pial surface	**Left hemisphere**	**Right hemisphere**
25%	Superior parietal (3) - precentral (2) – inferior parietal (2) – rostral middle frontal (2) – pars triangularis (1) – caudal middle frontal (1) – cuneus (1) – precuneus (1) - supramarginal (1)	Inferior parietal (2) – precuneus (2) – cuneus (1) – lateral occipital (1) – lingual (1) – peri-calcarine (1) -
50%	Precentral (3) – superior temporal (1) – superior parietal (1) – cuneus (1) – supramarginal (1) – caudal middle frontal (1)	Superior frontal (1) – precuneus (1) – precentral (1)
75%	Superior parietal (1) – superior temporal (1) - inferior parietal (1)	Caudal anterior cingulate (1)
Positive correlation		
Cortical depth - distance from pial surface	**Left hemisphere**	**Right hemisphere**
25%	Isthmus cingulate (1)	Caudal anterior cingulate (2) – isthmus cingulate (1) – superior frontal (1)
50%	Isthmus cingulate (2) – postcentral (1)	Postcentral (3) – caudal anterior cingulate (2) - supramarginal (2) – precuneus (1) – pars opercularis (1) –insula (1) – isthmus cingulate (1) – inferior parietal (1)
75%	Lateral occipital (4) – isthmus cingulate (2) – precentral (2) – precuneus (1) – posterior cingulate (1)	Postcentral (6) – precuneus (2) – caudal anterior cingulate (2) – supramarginal (2) – superior frontal (2) - rostral middle frontal (1) - pars opercularis (1) – middle temporal (1) – insula (1) – lingual (1) – lateral occipital (1) – precentral (1) – transverse temporal (1) – superior temporal (1) – inferior parietal (1)
SDMT-z		
Negative clusters		
Cortical depth - distance from pial surface	**Left hemisphere**	**Right hemisphere**
25%	Lateral occipital (1)	none
50%	Lateral occipital (1) – precentral (1)	Caudal anterior cingulate (1) – supramarginal (1)
75%	Precuneus (1) – precentral (1)	Caudal anterior cingulate (1) – supramarginal (1)
Positive clusters		

Cortical depth - distance from pial surface	Left hemisphere	Right hemisphere
25%	Pars triangularis (2) – superior parietal (2) – superior frontal (2) – rostral middle frontal (1) – pars opercularis (1) – superior temporal (1) – postcentral (1) – supramarginal (1)	Inferior parietal (3) – supramarginal (2) – superior parietal (1) – rostral middle frontal (1) – superior frontal (1) – precuneus (1) – lateral occipital (1) – peri-calcarine (1)
50%	Superior parietal (4) - rostral middle frontal (3) – pars triangularis (2) – caudal anterior cingulate (2) – superior frontal (2) – superior temporal (2) - pars opercularis (1) – precuneus (1) – supramarginal (1) – cuneus (1) – inferior parietal (1)	Inferior parietal (5) – lateral occipital (5) - supramarginal (2) – superior parietal (2) - lingual (2) – precuneus (2) – peri-calcarine (2) - post central (1) – superior temporal (1)
75%	Superior parietal (2) – rostral middle frontal (2) – superior frontal (1) – superior temporal (1) – supramarginal (1)	Inferior parietal (3) – lateral occipital (3) - supramarginal (2) – superior temporal (2) – postcentral (2) – superior parietal (2) - inferior temporal (1) – isthmus cingulate (1) – precuneus (1)

Discussion

In this study, we applied CME from quantitative 7T acquisitions to assess microstructural changes likely related to myelin content in cortical lesions and normal-appearing cortex of early MS cases. To exclude that CME changes could reflect other pathological factors including neurite/dendrite loss, NODDI measurements were also obtained. In patients, mean CME was overall abnormally decreased in cortical lesions and several regions of the cortical mantle, without significant changes in diffusion metrics or cortical thinning, suggesting early cortical demyelination in the absence of decreased neuroaxonal density and overt cortical atrophy. Individual cortical lesion analysis and the vertex-wise analysis, however, also revealed heterogeneous CME patterns, possibly reflecting underlying concomitant phenomena of complete demyelination, partial demyelination or remyelination, similarly evident at 1-year follow-up.

Although initially considered as a hallmark of progressive disease (Kutzelnigg et al., 2005), cortical demyelination has also been demonstrated in early MS by histopathological observation (Lucchinetti et al., 2011), where cortical demyelination was detected in 38% of subjects at disease onset, in some areas associated to meningeal inflammation. In the majority of cortical lesions, neurites were preserved, though neurite swelling was observed in few cases. Magnetic resonance imaging studies at lower field strength have also shown cortical demyelinating lesions in the very early stages of the disease (Calabrese et al., 2010; 2010b).

Visualization of cortical pathology thought to reflect myelin changes has been previously reported in vivo in early MS in focal cortical lesions segmented from 7T MRI acquisitions by applying the ratio of T1- and T2-weighted images (Granberg et al., 2017). This ratio combines the information from T2 and T1 signals, which show opposite correlations with myelin (negative for T2-, positive for T1-weighted sequences), thereby enhancing the contrast to noise ratio for myelin and providing a relatively simple and clinically feasible method to map cortical myelin content (Glasser and van Essen 2011; Glasser et al., 2016). Previous data provided evidence that this technique can detect cortical microstructural changes in early MS in vivo (Righart et al., 2017). The pathophysiological correlates of the T1/T2-weighted ratio in MS, however, remain uncertain. Analysis of T1/T2-weighted ratio values of ex vivo progressive MS brains yielded a strong correlation with dendrite density but not with myelin

(Righart et al., 2017), while other *post mortem* MS imaging data found that T1/T2-weighted ratio values significantly differ between demyelinated and non-demyelinated cortex (Nakamura et al., 2017). In our study, cortical CME in the healthy group correlated across several Brodmann areas to myelin optical measurements obtained from histology, providing indirect evidence that the metric reflects, at least partly, changes related to cortical myelin content.

In our cohort, cortical lesions were present in 80% of MS subjects, confirming high in vivo detection of cortical pathology in early MS by 7T MRI (Pitt et al., 2010; Kilsdonk et al., 2016; Granberg et al., 2017).

Overall CME was reduced both in cortical lesions and normal-appearing cortex, suggesting the presence of widespread microstructural abnormalities likely related to demyelination. When we performed an individual cortical lesion analysis, we found that 60% of cortical lesions had some degree of demyelination while the remaining had reduced CME in less than 5% of the total voxels. These findings, also present at vertex-wise level in the normal-appearing cortex, would suggest the presence of concomitant phenomena of incomplete demyelination and, possibly, remyelination. This pattern is supported by previous combined histopathological/MRI analyses of autoptic cortical MS tissue, which showed that some of the cortical hyperintensities detected by 7T T2* sequences (7/83, 8%) represented incompletely demyelinated or remyelinating areas (Kilsdonk et al., 2016).

As reported in histology works, remyelination in the MS cortex could be extensive and widespread (Albert et al., 2007; Strijbis et al., 2017). These studies provided evidence that remyelination, either extensive or partial, is present in the majority (more than 70%) of cortical lesions in chronic MS (Albert et al., 2007; Strijbis et al., 2017).

It is also known though that the newly formed myelin sheaths are usually thinner than those that never underwent demyelination. Their chemical composition, however, might be different, and other factors including iron deposition, reduction of axon density, or the presence of inflammatory cells (Patrikios et al., 2006; Haacke et al., 2009; Lee et al., 2019), might be influencing our measurements.

Longitudinal data showed an overall decrease of CME values both in cortical lesions and normal appearing cortex. The GLM analysis showed the presence of areas of both reduced and increased CME when comparing the whole cortex in MS patients at baseline and 1-year follow-up. Remyelination and demyelination in MS are dynamic processes, alternating and

coexisting within the same subject, its extent varying based on intrinsic factors, the anatomical location and the disease phase (Patrikios et al., 2006, Albert et al., 2007; Bramow et al., 2010; Strijbis et al., 2017).

At follow-up, we found remyelinating lesions in 4/10 MS subjects, within 16% of total lesions. Pathology showed that about 18% of cortical lesions are extensively remyelinating in chronic MS (Albert et al., 2007).

The results from the NODDI analysis showed that neither NDI nor ODI were pathological in patients, while CME showed significant differences both in cortical lesions and in normal-appearing cortex, proving to be more sensitive in disclosing early microstructural damage.

The NDI relates to neuroaxonal density and has been found to be reduced in the MS white matter and cortical lesions from the disease stages (Granberg et al., 2017; Grussu et al., 2017). Our results suggest that, at least in our cohort, cortical demyelination is not accompanied by neural loss in the early phase of the disease, as previously observed by *ex vivo* analysis of the MS cortex (Lucchinetti et al., 2011).

In *ex vivo* studies, NDI has been also found to correlate with myelin content (Jespersen et al., 2010, Grussu et al., 2017). Our results suggest that, at least in our cohort, CME represents a more sensitive measure of cortical microstructural changes likely related to demyelination, especially in the early MS stages when myelin pathology might not be necessarily accompanied by a decrease in neuroaxonal density. Additionally, relative to NODDI, the CME approach from 7T MRI enables acquisition of higher resolution images, which may be more effective for laminar cortical pathology analysis.

The higher ODI found in cortical lesions with increased CME at follow-up could indicate higher arborization of the dendrites in repairing lesions, as opposed to the lower arborization found in demyelinating lesions (Zhang et al., 2012; Grussu et al., 2017). We cannot completely rule out, however, that the increase in CME observed at follow-up could have been, at least in part, influenced by resolution of possible inflammatory processes within cortical lesions (Herranz et al., 2019).

We did not observe significant changes in cortical thickness, cortical volume or lesion load after 1 year, but detected significant changes is CME. This indicates the presence of ongoing microstructural cortical damage present since the early phase of the disease, detectable by quantitative imaging, which represents a more sensitive tool than anatomical MRI.

Neurological disability as measured by EDSS showed both negative and positive clusters of correlation with CME. Negative clusters along the precentral gyrus can indicate an effect of demyelination on cortico-spinal tract integrity, which has been reported to be affected from the early stages of the disease (Pawlitzki et al., 2017).

Information processing speed scores positively correlated with CME in several regions, especially in the superior parietal lobule, inferior parietal lobule, lateral occipital cortex, lingual gyrus and supramarginal gyrus. These areas are involved in visual orientation, object recognition and visual memory. The SDMT is typically used to test processing speed in patients with MS. Processing speed is mainly guaranteed from the integrity of several white matter tracts, although the presence of lesions in specific cortical regions, in particular Brodmann areas 39 and 40, has been proved to affect it (Turken et al., 2008).

The finding of both positive and negative correlation, however, is probably due to the low disability in our early cohort and the pretty homogeneous EDSS scores among subjects, which affected the statistical power of the analysis. However, the presence of both negative and positive clusters may, at least in part, indicate the presence of heterogeneous microstructural alterations in which areas of demyelination and remyelination coexist. These phenomena of remyelination do not seem to necessarily have a positive effect on clinical outcome. As suggested from a study on animal models, remyelination itself can alter cortical circuits, possibly leading to functional impairment (Orthmann-Murphy et al., 2020). Cortical microstructural damage can directly affect cognitive and sensorimotor domains and cause disability. However, our results suggest that CME changes are not necessarily associated topographically to functional impairment. The presence of cortical demyelination and compensatory remyelination instead should be considered as an index of severity of the disease, at least in our early MS cohort. In this scenario, SDMT proved to relate to cortical demyelination better than EDSS, although this has to be validated by more systematic analyses. Cognitive impairment in MS can occur during the early phases and is often underdiagnosed, being already present when physical disability is still minimal (Anhoque et al., 2012; Menascu et al., 2019).

We observed an area of increased CME, suggesting higher myelin content, when comparing the patient group versus control group, in the right caudal anterior cingulate (figure 1.5 C). Interestingly, this area of increased CME positively correlates with EDSS scores and negatively with cognitive performance. This could indicate that, in this case, cortical

remyelination represents a reaction to massive demyelination related to more aggressive forms of the disease, but it is not sufficient to compensate for clinical disability.

On the other hand, data from PET imaging show that remyelination in the white matter is more favourably related to disability outcomes in MS (Bodini et al., 2016). The biological mechanisms connecting cortical remyelination and clinical outcome in MS patients are, however, still to be elucidated, as well as the extent to which cortical remyelination contributes to improving disease course. Our study included an MS cohort with relatively low disability scores and short disease durations. It is possible that more significant effects of demyelination on clinical status might manifest later as the disease progresses. Further studies on later and progressive MS stages, as well as longitudinal examinations, could help to clarify this aspect. Longitudinal studies can also establish the value of cortical demyelination assessment for predicting the occurrence of cognitive disability and other neurological impairment.

Cortical CME in the control group correlated across several Brodmann areas to myelin optical measurements obtained from histology (Braitenberg 1962), providing indirect evidence that the metric is related to cortical myelin content. Compared to previous CME data obtained by combining 7T T2* with 3T magnetization transfer ratio (Mangeat et al., 2015), the current approach enables acquisition of higher resolution images, more effective for laminar cortical pathology analysis (Mangeat et al., 2018).

Limitations to our study include the small follow-up sample that might have affected the statistical power to investigate further longitudinal changes in cortical CME, as well as the lack of longitudinal data for healthy subjects, although high scan-rescan reproducibility of CME in healthy subjects was previously demonstrated (Mangeat et al., 2018). Although we provided indirect validation of the technique, an *ex vivo* study is further required to completely clarify the reliability of our measurements, especially in lesioned tissue, where other factors aside myelin content, including inflammation, might influence our metric.

In conclusion, our study showed that CME using ultra high resolution quantitative T2* and T1 at 7T is a sensitive technique to detect early cortical microstructural changes in early MS likely related to concomitant processes of cortical demyelination and remyelination. The correlation to clinical disease burden, at least in the early phase of MS, showed ambivalent results. Further investigations involving patients at later stage of the disease, a larger cohort

and longer follow-up are required to better clarify the nature of cortical demyelination and remyelination and their relationship to the disease outcome.

The quantitative approach proposed in this study could be also applied to investigate other neurological diseases affecting the cortex, like dementia, epilepsy and cerebrovascular disease.

Section 2

Characterization of inflammatory disease activity and its relation to myelin content in the lesioned and normal-appearing white matter in patients at different stages of multiple sclerosis: a combined MR-PET and synthetic MRI study

Summary

Objectives. To assess neuroinflammation in the white matter lesions and normal-appearing white matter of patients with different subtypes of MS (relapsing-remitting and secondary progressive) by ^{11}C-PBR28 PET imaging; to relate inflammatory activity to clinical and radiological disease burden; to classify white matter lesions based on their inflammatory activity relative to normal-appearing white matter; to assess myelin content in the lesioned and normal-appearing white matter by synthetic MRI imaging and correlate it to neuroinflammation and disease burden.

Methods. Patients with MS and healthy volunteers were scanned in a 3 Tesla MR-PET scanner after injection of ^{11}C-PBR28 for quantification of microglia activation. The synthetic MRI protocol was acquired in the same session. White matter lesions were segmented on 3 Tesla FLAIR or 7 Tesla T2* sequences. Clinical disability was assessed in MS patients by EDSS and SDMT scores. White matter ^{11}C-PBR28 binding was assessed using standardized uptake values (SUV). To account for global signal differences across subjects, SUV maps were normalized by a pseudo-reference region (SUVR) in the normal-appearing white matter with mean SUV in patients around the mean SUV in controls. Myelin content maps were obtained automatically by the synthetic MRI software. Values of SUVR and myelin content were obtained for white matter lesions, perilesional areas and normal-appearing white. SUVR values were compared in MS and healthy controls by voxel-wise analysis on FSL. The relative differences in tracer uptake between patients and controls was used to extract a threshold for differentiation active versus non-active patients, depending on the inflammatory activity in their white matter lesions. White matter lesions were classified, based on their TSPO uptake relative to the surrounding white matter, in active, peripherally active and inactive. Correlations between SUVR and myelin content were assessed in white matter lesions, perilesional areas and normal-appearing white matter. Values of SUVR and myelin content were also related to clinical and radiological parameters.

Results. The voxel-wise analysis revealed the presence of high inflammatory activity in the white matter of 33 MS patients compared to 16 healthy controls. Patients classified as active based on their white matter lesion inflammation had longer disease duration and worse

disease outcomes compared to non-active subjects. SUVR values in white matter, perilesional areas and normal-appearing white matter correlated with clinical and radiological metrics.

Active white matter lesions were more frequent in the early disease and decreased with disease duration, while inactive lesions showed inverse behaviour. Peripherally active lesions were more frequent in the secondary progressive disease and related to clinical disability.

Myelin content inversely correlated with microglia activation especially in white matter lesions and directly correlated with clinical and radiological disease burden.

Conclusion. Our study confirmed an increased microglia activation in MS patients versus healthy subjects, which relates to clinical and radiological outcomes. Myelin content inversely correlates with microglia activation especially in white matter lesions and with clinical and radiological disease burden. The synthetic MRI proved to be a useful tool to assess pathological myelin changes in MS and a promising tool for monitoring the effect of myelo-protective and remyelinating drugs.

Introduction

2.1 Classification of MS lesions based on inflammatory activity

Several pathological classifications of MS lesions have been proposed in the last decades (Trapp et al., 1998; Lucchinetti et al., 2000; Kuhlmann et al., 2017). These classifications are based on the presence of factors as cell infiltration (lymphocytes, macrophages/microglia), astrogliosis, axonal loss, myelin loss and myelin degradation products inside the macrophages/microglia (fig. 2.1). These elements allow the staging of the lesion based on the inflammatory and the demyelinating activity.

Inflammatory *active lesions* with myelin destruction are more typical of the early MS phases, as shown in WML in an *ex vivo* study (Frischer et al., 2015), and decrease with disease duration. Inflammatory active lesions represent the initial appearance of established MS lesions and are the lesions which most likely will help to identify pathogenetic mechanisms contributing to lesion formation (Kuhlmann et al., 2017).

Peripherally active lesions are those in which the lesion core is inactive and the inflammatory activity is confined to the periphery. They may or may not show demyelinating activity. These lesions have also been called "smoldering" or "slowly expanding" when found in the later stages of the disease (Lassmann 2008; Frischer et al., 2015; Seti et al., 2017).

Inactive lesions are hypocellular and feature marked axonal loss. A gliotic scar of astrocytes can be present (Ludwin 2000). Inactive lesions are the dominating type in MS patients with long disease duration and/or SPMS without attacks (Frischer et al., 2015).

Remyelination, detected in all lesion types described, can be defective especially in patients with progressive disease. Extensive remyelination can be found in about 20% of lesions (the so-called "shadow plaques"), although the newly formed myelin can be instable and undergo new waves of demyelination (Patrikios et al., 2006; Bramow et al., 2010). As previously discussed, the efficacy of remyelination depends on lesion location, as well as intrinsic factors related to the patient (Patrikios et al., 2006; Albert et al., 2007; Goldschmidt et al., 2009; Strijbis et al., 2017).

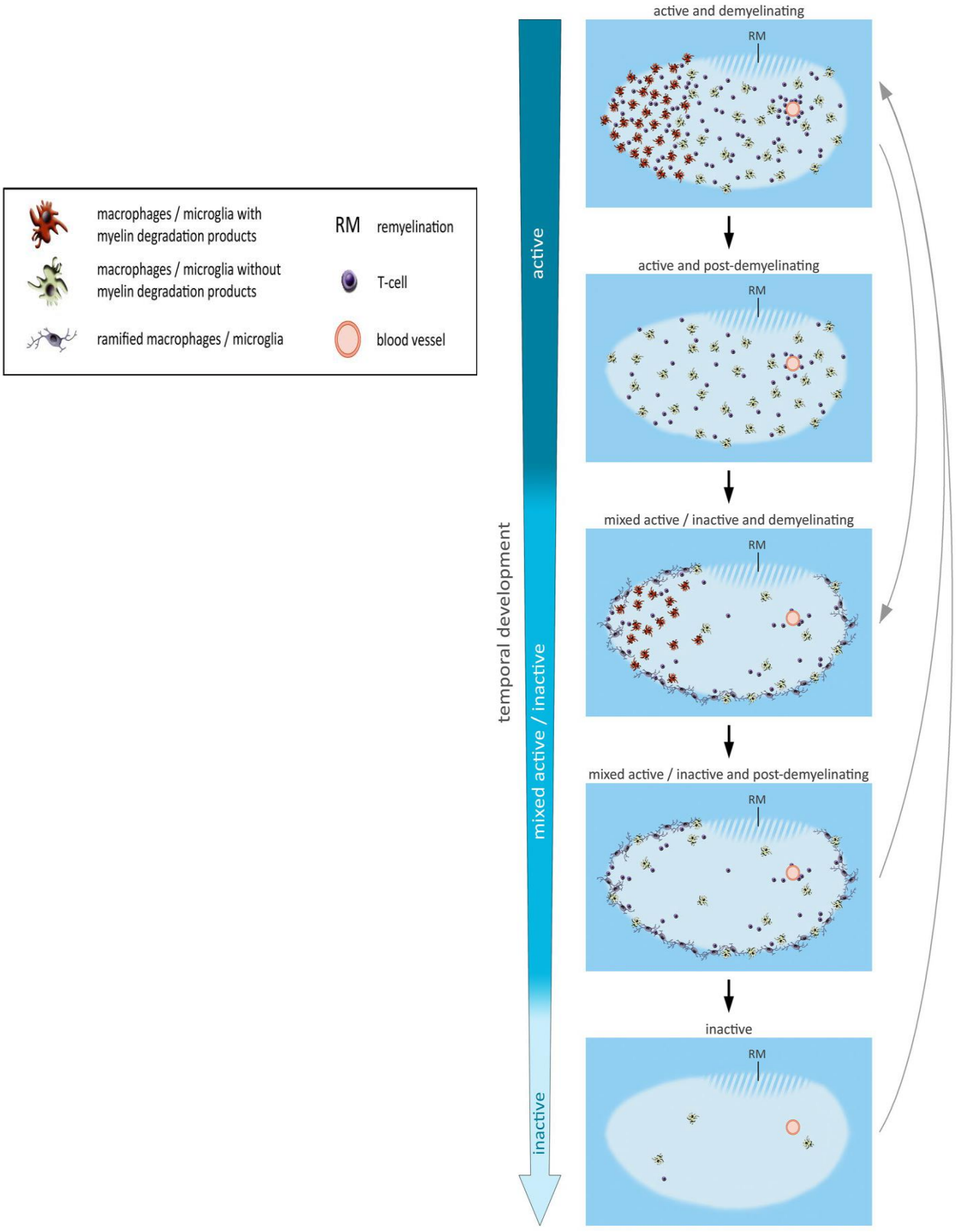

Fig. 2.1. schematic representation of MS lesions based on lesion aging, inflammatory activity and demyelination activity (from Kuhlmann et al., 2017).

2.2 *In vivo* characterization of MS lesion types

Imaging studies have recently focused on the characterization of the inflammatory activity of MS lesions and their relation to clinical disability and disease course.

A positron emission tomography (PET) study with ^{11}C-PBR28, a marker of activated microglia, detected *in vivo* the presence of inflammatory active lesions in the white matter of both SPMS and RRMS patients, although more frequently in the second group, a higher proportion of inactive lesion in the progressive disease and an association of this type of lesion with disease duration. Active lesions were detected also in treated patients (Datta et al., 2017).

In another PET study with the same radiotracer, we proved the presence of active versus non-active lesions in cortical grey matter (Herranz et al., 2020). ^{11}C-PBR28 uptake was abnormally high in cortical lesions in RRMS and SPMS; in SPMS, tracer uptake was significantly increased also in normal-appearing cortex. Patients with high cortical lesion inflammation had worse clinical outcome and higher intracortical lesion burden than patients with low inflammation.

In an ultra-high-field MRI study, the presence of expanding lesions in the white matter has been associated with a more aggressive disease course, even in individuals on highly effective MS treatment (Absinta et al., 2019).

2.3 Visualization of MS inflammatory activity by ^{11}C-PBR28 PET

Activated microglia upregulate the expression of the 18kDa mitochondrial translocator protein (TSPO), which can be imaged *in vivo* by selective PET TSPO radioligands (Banati et al., 2000). A genetic polymorphism of the TSPO rs697 gene, leads to three possible binding affinity patterns: high, mixed and low (Owen et al. 2012).

In previous studies, using MR-PET imaging with ^{11}C-PBR28, a second-generation TSPO radiotracer, we demonstrated abnormally increased cortical TSPO expression, indicative of microglia activation, in a cohort of MS patients relative to a healthy control population matched for binding affinity and age, in normal-appearing white matter (NAWM), cortex, thalamus, hippocampus and cerebellum (Herranz et al., 2016, Barletta et al., 2020). In these patients, microglia activation correlated with clinical disability. Interestingly, in contrast to WM plaques, where ^{11}C-PBR28 uptake was greater in SPMS than in RRMS, cortical lesions showed similar levels of abnormally high TSPO expression in both disease stages. We also found that, especially in RRMS, neuroinflammation was not strictly associated with MRI metrics of neurodegeneration. Importantly, in cases where post-gadolinium contrast agent

scans were available, cortical microglia activation was not accompanied by the presence of macroscopic disruption of the blood brain barrier.

2.4 Quantification of myelin content by a new synthetic MRI approach

The water entrapped between the myelin sheaths has specific physical properties with rapid relaxation times (~10 ms), due to its strong magnetization exchange with the myelin macromolecules. This phenomenon makes visualization of bound myelin water by conventional MRI methods challenging. Recently, a new MRI myelin detection model was proposed to measure the presence of myelin by its effect on the surrounding cellular water (Warntjes et al., 2016, Granberg et al., 2016). The observable relaxation rates of cellular water increase in the vicinity of myelin due to magnetization exchange with fast-relaxing myelin water. Meanwhile, the observable proton density decreases in the presence of myelin, since the myelin water decays too fast to be detected by conventional imaging. These effects are used for myelin visualization using a multi-parametric MRI acquisition that quantifies R1 and R2 relaxation rates (the inverse of the corresponding relaxation times T1 and T2) and the proton density. The concept of this method is incorporated in the Rapid Estimation of Myelin for Diagnostic Imaging (REMyDI) featuring the post-processing framework of the Synthetic MRI (SyMRI) software (https://www.syntheticmr.com).

In a recent study, this promising technique showed a reduction in myelin content in the NAWM in MS patients versus controls, and a correlation with physical disability in the longitudinal observation (Ouellette et al., 2020; figure 2.2).

Figure 2.2. T2-weighted fluid-attenuated inversion recovery and the corresponding rapid myelin imaging in 4 representative subjects. A) A 56-year-old female healthy control. B) A 53-year-old female with primary progressive multiple sclerosis, disease duration of 9 years, EDSS score of 3.5, SDMT z score of −0.38. C) A 39-year-old female with relapsing–remitting multiple sclerosis, disease duration of 14 years, EDSS score of 1.0, SDMT z score of −1.0. D) A 40-year-old female with secondary progressive multiple sclerosis patient, disease duration of 25 years, EDSS of score 7.0, and SDMT z score of −3.9. (from Ouellette et al., 2019).

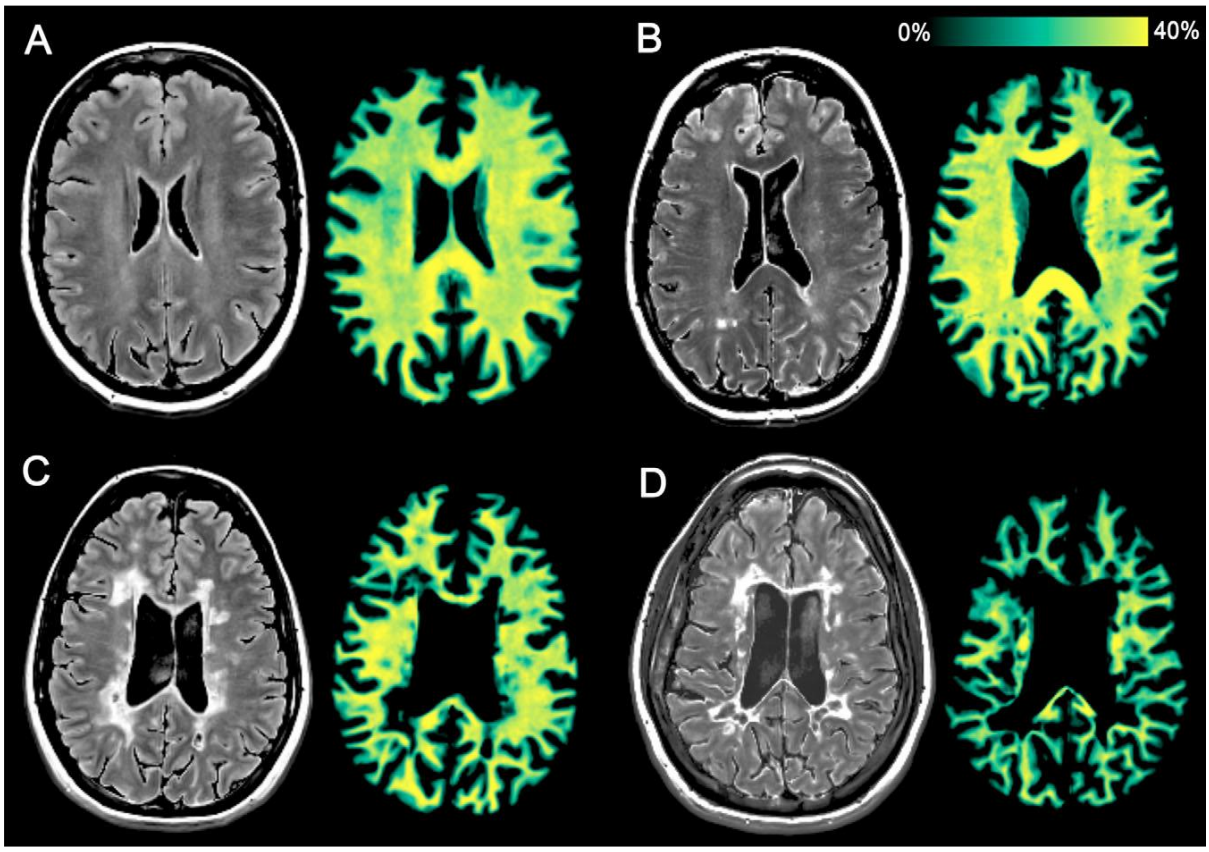

2.5 Hypothesis and aims

In this combined PET-MRI study, we aimed at classifying patients with MS at different stages in active versus non-active based on the presence of ^{11}C-PBR28 tracer uptake, indicating microglia activation, in the white matter lesions. Successively, we assessed the differences between the two groups in MRI and clinical disease burden. We also aimed at performing a classification of white matter lesions based on their inflammatory activity relative to surrounding normal-appearing white matter in different MS subtypes, as recently proposed by other *in vivo* imaging studies.

We hypothesized that myelin content in the white matter of MS patients can be influenced by the presence of inflammatory activity. To address this hypothesis, we applied synthetic MRI techniques to quantify myelin content in lesions and non-lesioned white matter and correlated it to microglia activation. We also correlated myelin content in the white matter lesions and surrounding normal-appearing white matter to clinical and radiological metrics.

Methods

2.6 Subjects and clinical assessments

The Institutional Review Board approved this prospective cohort study protocol, and subjects gave written informed consent to participate in the study. General inclusion criteria were: age 18-60 years, no significant medical history (other than MS for patients), absence of MRI contraindications, high- or mixed- affinity binding for ^{11}C-PBR28. Eligibility criteria for MS subjects were: diagnosis of MS according to the McDonald criteria (Polman et al., 2011), stable disease-modifying treatment or no treatment for at least 3 months, no relapses in the 3 months prior to enrolment, no corticosteroids use for at least 1 month prior to enrolment.

All MS patients underwent a neurological examination with assessment of Expanded Disability Status Scale (EDSS) score and Symbol Digit Modalities Test. One patient could not perform SDMT because of severe visual impairment. Symbol Digit Modalities Test raw scores were converted to z scores (SDMT-z) after correcting for age and years of education (Parmenter et al., 2010).

2.7 MRI protocol

All study subjects underwent a 90-minute ^{11}C-PBR28 MR-PET imaging on a Siemens integrated 3T MR-PET system (BrainPET), with a spatial resolution of ~2.8 mm in the center of the field of view. PET data were acquired after receiving an intravenous bolus injection of ^{11}C-PBR28 produced in-house (Herranz et al., 2016 and 2020). For generation of attenuation correction maps, MPRAGE images were acquired simultaneously to PET. A fluid attenuated inversion recovery (FLAIR) sequence for white matter lesion segmentation was acquired in those subjects in which 7 Tesla images were not available.

In a subgroup of MS patients, a synthetic MRI sequence was obtained for quantification of white matter myelin content: imaging parameters were axial field of view of 230 × 184mm, voxel size of 0.9 × 0.9 × 3.0mm3 with a 0.5 distance factor, 30 to 34 slices (to ensure full intracranial coverage), repetition time of 4,260 milliseconds, echo times of 22/100 milliseconds, effective inversion times of 150/580/2,000/4,130 milliseconds, flip angle of 120°. The synthetic MRI was used to generate the quantitative maps, T1-weighted images (repetition time = 500 milliseconds, echo time = 10 milliseconds), and T2-weighted fluid

inversion recovery images (repetition time = 15,000 milliseconds, echo time = 100 milliseconds, inversion time = 3,000 milliseconds).

The image acquired at 7T for white matter lesion segmentation consisted of a single-echo T2*-weighted spoiled gradient-echo pulse sequence (resolution = 0.33 × 0.33 × 1 mm^3, 25% gap).

Figure 2.3 summarizes the MRI acquisition and analysis procedures of the study.

2.8 Quantification of ^{11}C-PBR28 binding

White matter ^{11}C-PBR28 binding was assessed using standardized uptake values (SUV). In-house software was used to compute voxel-wise, for each subject, SUV (mean radioactivity/injected dose/weight) from the 60–90 minutes post-injection data (Herranz et al., 2016). PET data were reconstructed using 3D ordinary Poisson ordered subset expectation maximization reconstruction, with corrections for attenuation, scattering, random coincidences, dead-time, sensitivity, and normalization.

To account for global signal differences across subjects, SUV maps were normalized by a pseudo-reference region (SUVR) in normal-appearing WM with mean SUV in patients around the mean SUV in controls. It has been demonstrated that SUVR estimated with this method strongly correlate with the volume of distribution of the same tracer (Herranz et al., 2016).

2.9 Quantification of myelin content

The REMyDI myelin quantification is based on the R1, R2, and PD maps, where each voxel is modeled into 4 compartments—the myelin, cellular, free water, and excess parenchymal water partial volumes (Warntjes et al., 2016). The myelin partial volume has very fast relaxation rates and is not directly measurable but is instead estimated through its magnetization exchange and effect on the observable proton pool. The REMyDI myelin maps were generated automatically in SyMRI.

2.10 White matter lesion segmentation and analysis

White matter lesions were manually segmented by consensus of two experienced raters on Slicer (v4.2.0) on 3T FLAIR images or 7T T2* images. Individual lesion masks were extracted

by in-house script in Matlab. Perilesional areas were obtained by enlarging the lesion masks by 3 mm and successively subtracting the original lesion masks from the enlarged by FSL.

Lesion and perilesional masks were registered to PET space and to the SyMRI space. Masks of NAWM were obtained subtracting the lesion and perilesional masks from automatic WM segmentation obtained by the synthetic MRI software processing (for SyMRI space) and from FreeSurfer (for PET space). Finally, values of myelin content (MyC) and SUVR were extracted from WML, perilesional areas and NAWM.

Lesion volumes were quantified by FSL using fslstats from FMRIB Software Library, v.5.0 (http://fsl.fmrib.ox.ac.uk/fsl).

2.11 Classification of MS patients based on inflammation in white matter lesions

The presence of significant differences in TSPO uptake in the white matter in MS patients versus controls was assessed by voxelwise analysis using FSL Randomise. Clusters in which SUVR values were higher in MS patients than in HC were obtained by this analysis. The percentage difference in SUVR in patients and controls within the clusters was estimated, separately for mixed affinity and high-affinity binders and used as threshold applied to each MS patient's uptake in the WML. The median volume of active WML was calculated voxel-wise in the whole MS cohort and used to group patients into two categories: (1) high inflammatory lesion activity, if the total volume of active cortical lesions in that individual MS patient was greater than or equal to the median and (2) low inflammatory lesion activity, if lower than the median. The two groups were then compared to assess the presence of differences in clinical and MRI metrics (EDSS, SDMT-z, disease duration, disease type, age at disease onset, WML volume).

2.12 Assessment of white matter lesion uptake relative to normal-appearing white matter

To account for individual variability in the tracer uptake and the innate inflammatory phenotype of each subject, SUVR in WML were also compared to values in NAWM. On the basis of test–retest PET data obtained from a subgroup on 16 patients in three different regions of interest (table 2.1), lesions were classified in three categories, based on the presence of differences in SUVR greater than 6.21% in the lesion core and in the perilesional area relative

to the surrounding NAWM: *active lesions*, with higher uptake than NAWM, *peripherally active lesions*, with higher uptake in the perilesional volume, and *inactive lesions*, with lower uptake than NAWM in the lesion and the perilesional area (Datta et al., 2017).

The percentage volume of active, inactive and peripherally active lesions relative to total WML volume was assessed for all subjects, related to disease duration and compared in RRMS and SPMS patients.

Myelin content was assessed in the three different types of lesions.

Table 2.1. Percentage change in SUVR for scan-rescan acquisitions in 16 MS patients. Mean follow-up time was 3.5±0.8 months.

Region of interest	percentage change
Normal-appearing white matter	6.21%
Cortical grey matter	5.12%
White matter lesions	5.81%

2.13 Statistical analysis

The demographic and clinical characteristics of the study subjects were analyzed by Wilcoxon test for non-parametric data, unpaired t test for normally distributed data and Fisher's exact test for categorical variables.

Differences in TSPO uptake between patients and healthy controls were assessed voxel-wise by Randomise, a tool for nonparametric permutation inference on FSL (https://fsl.fmrib.ox.ac.uk/fsl/fslwiki/Randomise). For our analysis, we used a Threshold-Free Cluster Enhancement and 500 permutations. Age and binding affinity were included in the model as confounding factors.

Differences in SUVR values were assessed in WML, perilesional areas and NAWM in MS patients by matched pairs t test.

Multilinear regression models were used to correlate SUVR values and WML inflammatory phenotype to clinical scores (age and binding affinity were included in the model as needed). Wilcoxon test compared the percentage of active, inactive and peripherally active lesions in RRMS versus SPMS patients, while the correlation between lesion inflammatory phenotype and disease duration was assessed by Spearman's test.

Pearson’s correlation was used to relate SUVR values in the WML, perilesional areas and NAWM.

Multilinear regression, including age as confounding factor, was used to relate MyC in the three regions of interest to EDSS. Spearman’s correlation was used to correlate MyC to SDMT-z, disease duration and WML load.

Intra-subject correlation in MyC in WML, perilesional areas and NAWM was assessed by Pearson’s or Spearman’s, based on data distribution.

Values of SUVR and MyC in WML, perilesional areas and NAWM were related by Spearman’s correlation.

MyC in the three WML types was compared by matched pairs t test.

Figure 2.3. Methodology of image acquisition and analysis. White matter lesions were segmented on 7 Tesla T2* or 3 Tesla FLAIR sequences. Maps of normalized uptake values (SUVR) were obtained by PET acquisitions reconstructed on MEMPRAGE 3-Tesla images. The 3-Tesla Synthetic MRI protocol included the acquisition of T2-weighted, T1-weighted and proton density sequences, which were processed to obtain maps of myelin content.

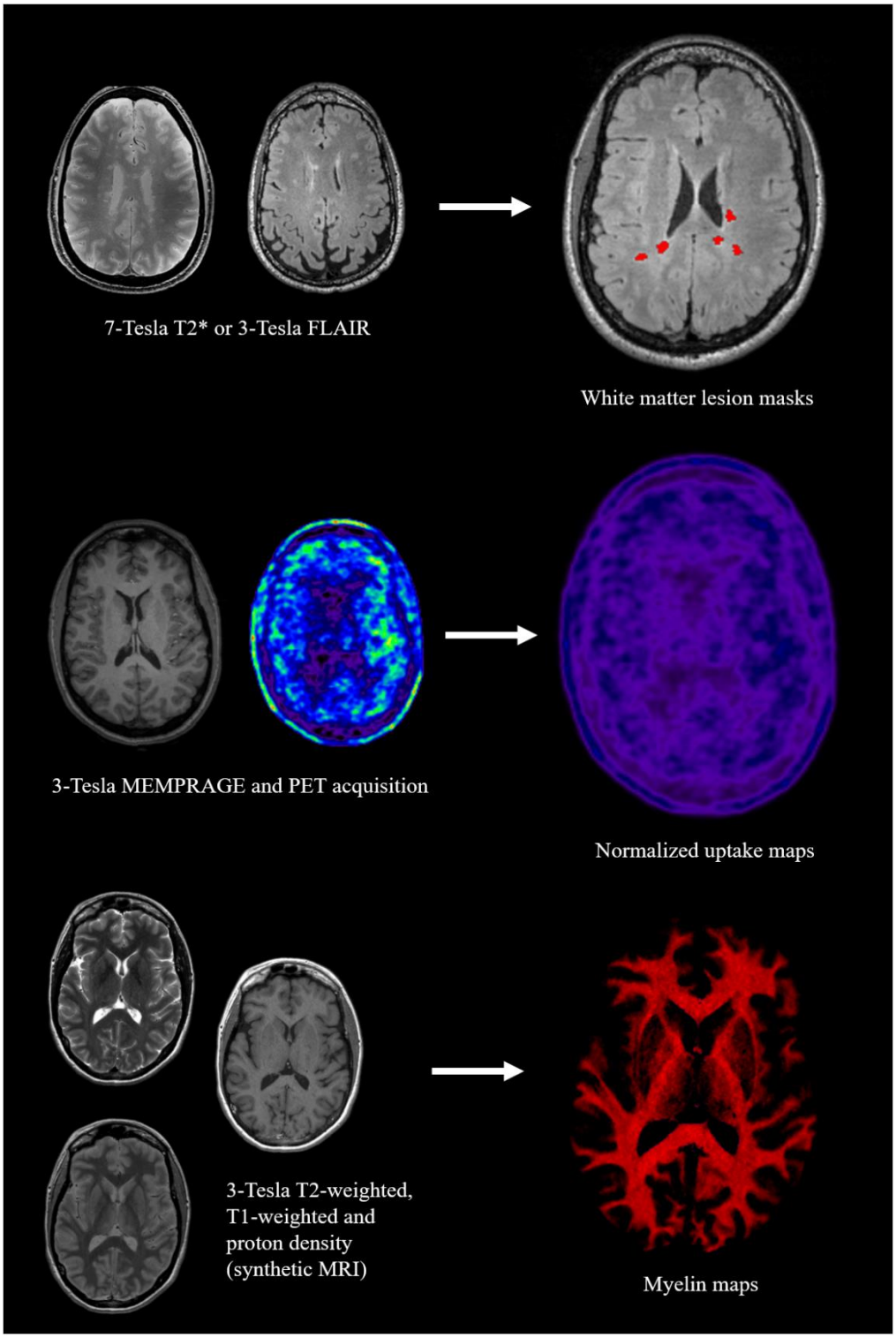

Results

2.14 Subjects

Table 2.2 summarizes the demographic and clinical characteristics of the subjects included in the study. Thirty-three patients with MS (13 RRMS and 20 SPMS) and 16 age- and gender-matched healthy volunteers were included in the analysis.

Table 2.2 Demographic and clinical characteristics of the study subjects.

Characteristic	**HC**	**MS all**	***P* value HC vs MS**	**RRMS**	**SPMS**	***P* value RRMS vs SPMS**
Number of subjects	16	33	-	13	20	-
gender F	11	24	1**	10	14	*1***
age in years mean±SD	47.6±12.2	49.9±9.2	0.7*	44.6±10.7	53.3±6.3	*0.03**
genotype high affinity	8	21	0.5**	9	12	*0.7***
age at onset in years mean±SD	-	32.4±10.0	-	35.1±10.0	30.7±9.9	*0.4**
disease duration y median (range)	-	16 (1-42)	-	6 (1-31)	21.5 (7-42)	*0.0009**
EDSS median (range)	-	4 (0-7)	-	1.5 (0-5)	6 (2.5-7)	*<0.0001**
SDMT-z median (range)	-	-1.19 (-4.04, 1.61)	-	0.25 (-2.5, 1.02)	-1.5 (-4.04, 1.61)	*0.046**
MS treatment						
- **ocrelizumab**	-	9	-	7	2	-
- **tecfidera**	-	6	-	4	2	-
- **rituximab**	-	4	-	0	4	-
- **glatiramer acetato**	-	3	-	1	2	-
- **natalizumab**	-	2	-	0	2	-
- **fingolimod**	-	2	-	0	2	-
- **mycophenolate mofetil**	-	1	-	0	1	-
- **none**	-	6	-	1	5	-

*by Wilcoxon test; **by Fisher's exact test

2.15 Differences in ^{11}C-PBR28 uptake in MS patients versus controls

The voxel-wise analysis showed the presence of clusters in the white matter in which SUVR values were higher in MS patients compared to healthy controls (figure 2.4).

Figure 2.4. The voxel-wise analysis performed in the white matter by FSL (Randomise) shows clusters in which the SUVR values are significantly higher in MS patients compared to healthy subjects.

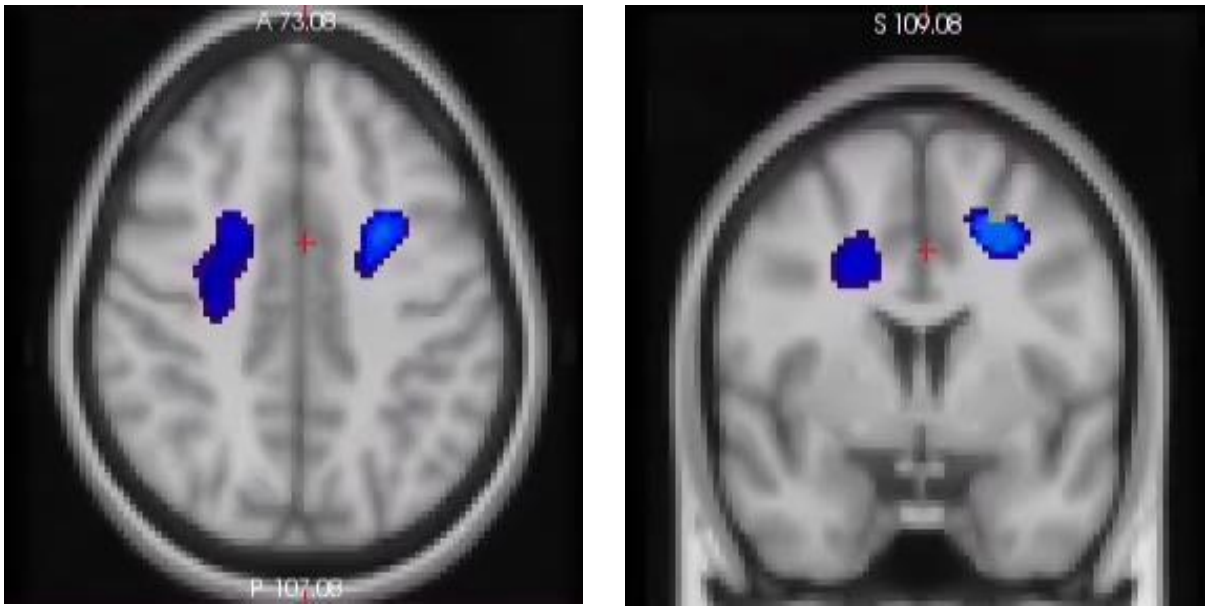

SUVR values were extracted from these clusters for patients and controls (table 2.3) and the thresholds for high- and mixed-affinity subjects were calculated as described in the methods.

Table 2.3. SUVR values within the clusters obtained by permutational analysis for patients and healthy volunteers, divided by binding affinity.

	MS patients	Healthy volunteers	Percentage difference
High binding affinity	1.113	0.960	16%
Mixed binding affinity	1.145	0.965	19%

2.16 Inflammatory activity in white matter lesions

The threshold obtained from the percentage difference in patients versus controls was applied to the WML to classify patients in active versus non-active. Sixteen MS patients (12 SPMS and 4 RRMS) had high inflammatory activity in the WML. These subjects, compared to the other patients, had longer disease duration, higher clinical disability and higher lesion load (table 2.4).

Table 2.4. Clinical and MRI characteristics of MS patients based on the inflammatory activity in the white matter lesions.

Characteristic	**Non-active patients**	**Active patients**	***P* value**
Number of subjects	17	16	-
age years mean±SD	47.1±10.5	52.8±6.8	*0.07**
disease duration years mean±SD	11.9±10.6	23.3±10.0	*0.04**
age at onset years mean±SD	35.2±10.2	29.4±9.1	*0.09**
disease type number of RRMS	9	4	*0.1***
EDSS mean±SD	3.1±2.0	5.2±2.0	*0.006**
SDMT mean±SD	-0.38±1.13	-1.61±1.56	*0.02**
WML mm^3 mean±SD	4009±5538	20698±18300	*<0.0003**

*by Wilcoxon; **by Fisher's exact test

2.17 Individual white matter lesion analysis

Active lesions were found in all 13/13 RRMS and 19/20 SPMS. Peripherally active lesions were found in 5/13 RRMS and 16/20 SPMS. Inactive lesions were found in all patients. The percentage of the total WML volume for each lesion type was assessed in RRMS and SPMS patients. Figure 2.5 shows the appearance of ^{11}C-PBR28 uptake in each type of lesion.

The percentage of active lesions tended to be higher in RRMS subjects (mean% ±SD 20% ±2 in RRMS, 9% ±1 in SPMS, *p=0.05* by Wilcoxon test), peripherally active lesions were higher in SPMS (2% ±0.3 versus 0.7% ±0.1 in RRMS, *p=0.04*), inactive lesions were proportionally higher in SPMS patients but the difference was not significant (89% ±1 versus 79% ±2 in RRMS, *p=0.2*).

The percentage of active lesions decreased with disease duration (p = 0.004, Spearman's rho =-0.48), inactive lesions increased with disease duration (p =0.006, rho =0.46), peripherally active lesion percentage did not correlate with disease duration (p = 0.6, rho =0.1).

Figure 2.5. Example of three different type of white matter lesions in a female patient with relapsing remitting multiple sclerosis, 54 years old, disease duration 6 years, EDSS 5, SDMT z score -2.27, treated with ocrelizumab. White matter lesion segmentation has been performed on 3 Tesla FLAIR sequences (left and center squares). The PET images (right squares, overlapped to FLAIR images) were normalized for a pseudo-reference region in the normal-appearing white matter, thus obtaining a map of standardized uptake values (SUVR, color bars). In the active lesion, an increase in tracer uptake can be seen in the lesion core. In the inactive lesion there is no detectable uptake. In the chronic active is it confined to the periphery of the lesion and the perilesional area.

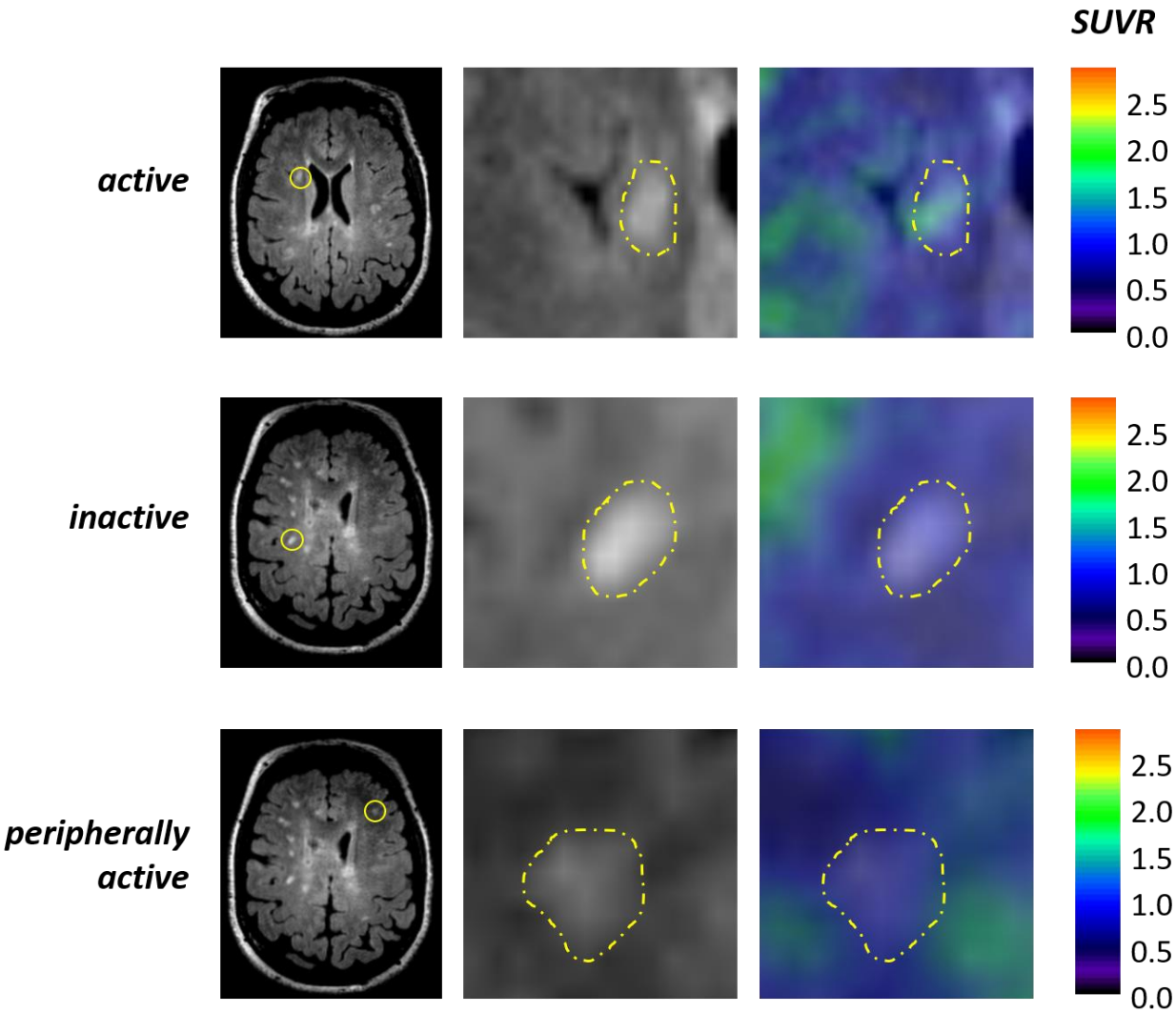

2.18 Correlation between SUVR and clinical and MRI metrics

Multilinear regression models showed correlations of EDSS, SDMT-z with SUVR values in the NAWM, in the perilesional areas and in the WML (figure 2.6).

A correlation was also found for WML load (with SUVR in NAWM, Spearman rho 0.48, p=0.0045; with SUVR in perilesional areas, Spearman rho 0.56, p=0.0008; with SUVR in WML, Spearman rho 0.51, p=0.0026).

Lesion load also correlated with EDSS (Spearman rho 0.53, p=0.001) and SDMT-z (Spearman rho -0.56, p=0.0007).

Figure 2.6. Multilinear regression assessing correlations between SUVR in WML, perilesional areas and NAWM and clinical metrics (EDSS, SDMT-z). Age and binding affinity were included as confounding factors.

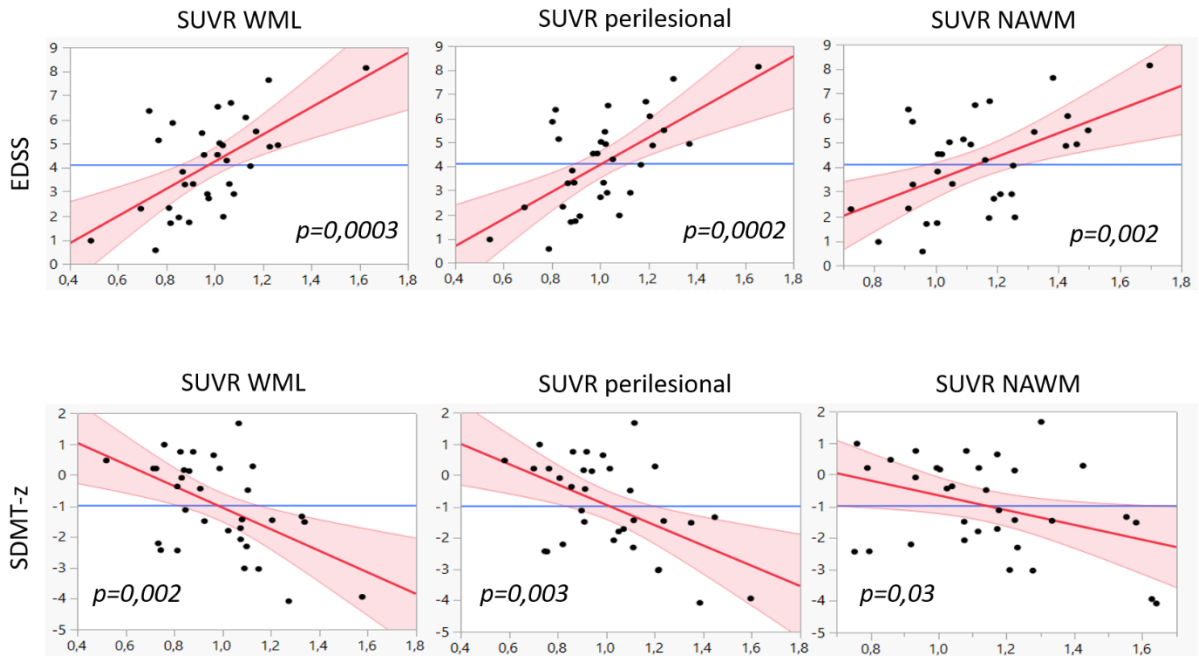

The number of peripherally active lesions correlated with EDSS (by multilinear regression, R^2 0.36, CCII 0.02-0.56, p=0.03, parameter estimate 0.29, total WML volume included as an adjusting factor) but not with SDMT-z. The number of active or inactive lesions did not correlate with clinical metrics.

2.19 Intra-subject variability of TSPO uptake

The TSPO uptake in the WML, in the perilesional areas and in the NAWM strongly correlate within the same patient: Pearson's analysis showed high correlation in the SUVR values between the three regions of interest in the MS cohort (figure 2.7).

Differences in SUVR values were assessed in WML, perilesional areas and NAWM in MS patients by matched pairs t test. The highest values were obtained for the NAWM, the lowest in WML. The uptake was significantly different for all the regions of interest (table 2.5).

Table 2.5. Uptake values in WML, perilesional areas and NAWM in MS patients.

SUVR WML mean±SD	0.98±0.22
SUVR perilesional mean±SD	1.01±0.23
SUVR NAWM mean±SD	1.14±0.24
T test WML vs NAWM	*p value <0.0001*
T test WML vs perilesional	*p value 0.0003*
T test perilesional vs NAWM	*p value <0.0001*

Figure 2.7. Pairwise correlation between SUVR values in the WML, perilesional areas and NAWM. Pearson's correlation is indicated in the graphs.

P value <0.0001
95% CCII 0.96-0.99

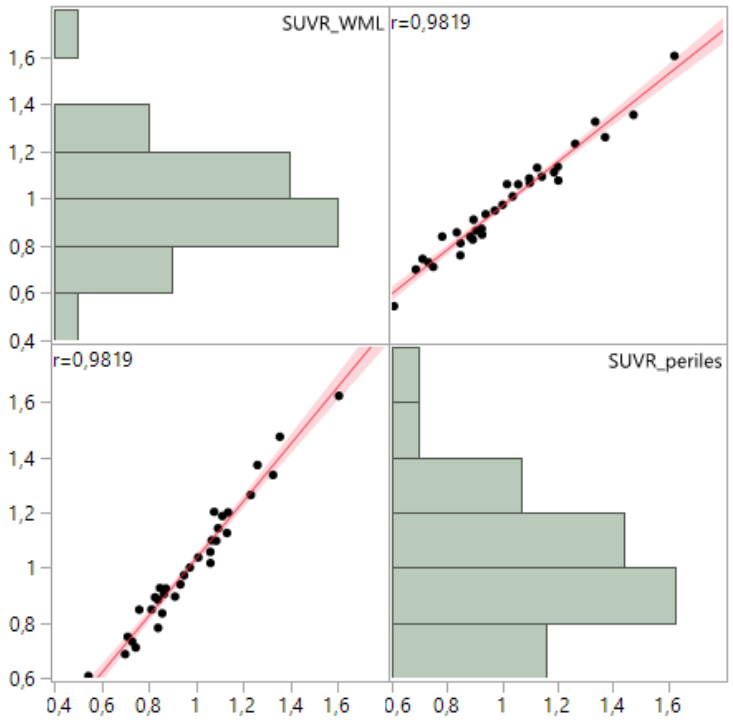

P value <0.0001
95% CCII 0.86-0.96

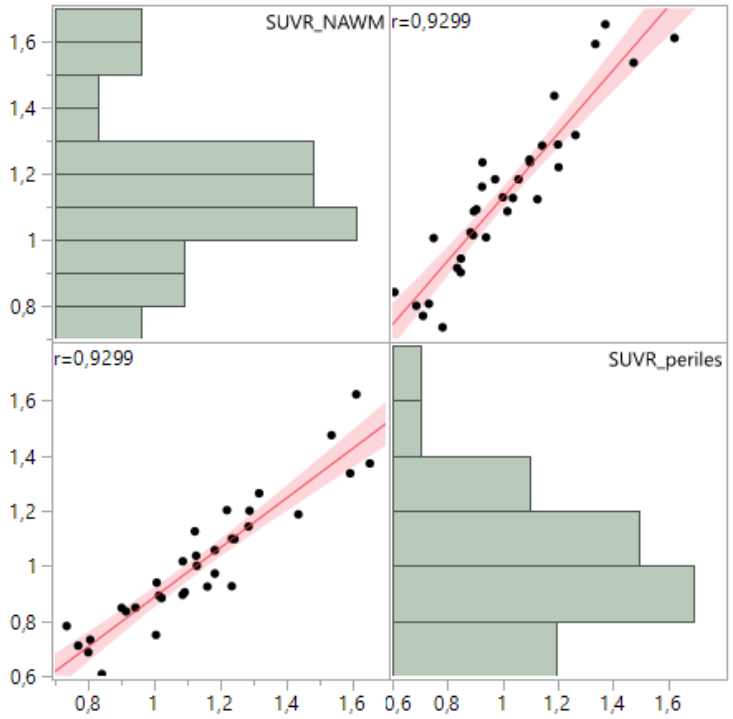

P value <0.0001
95% CCII 0.78-0.94

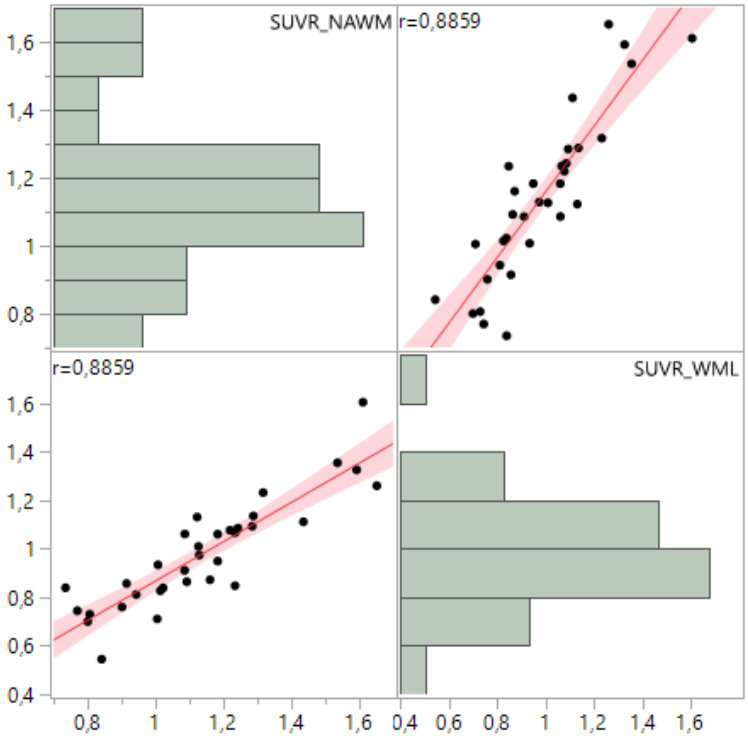

2.20 Synthetic MRI cohort – subjects

Eighteen subjects with MS were scanned for the acquisition of Synthetic-MRI images. Table 2.6 summarizes the characteristics of this MS population.

Table 2.6. Demographic and clinical characteristics of the synthetic-MRI subgroup.

Characteristic	all MS	RRMS	SPMS
number of subjects	18	13	5
age in years (mean±SD)	47.3±10.1	44.6±10.7	54.4±3.1
gender F/M	14/4	10/3	4/1
disease duration (mean±SD)	14.8±12	9.5±8.6	28.4±8.3
age at disease onset (mean±SD)	32.5±10.2	35.1±10	26±8.3
EDSS median (range)	2 (0-7)	1.5 (0-5)	5.5 (2-7)
SDMT-z median (range)	-0.46 (-2.98, 1.02)	0.25 (-2.5, 1.02)	-1.76 (-1.52, -2.98)
Treatment			
- **ocrelizumab**	9	7	2
- **dimethyl fumarate**	4	4	-
- **glatiramer acetate**	1	1	-
- **fingolimod**	1	-	1
- **rituximab**	1	-	1
- **mycophenolate mofetil**	1	-	1
- **none**	1	1	-

2.21 Correlation with clinical and radiological metrics

Myelin content (MyC) was extracted within WML, WM perilesional areas and NAWM for the two disease types (table 2.7) and related to clinical and radiological characteristics.

Patients with SPMS had lower MyC in the NAWM compared to RRMS. A trend was also found in the perilesional areas (figure 2.8).

Myelin content in the NAWM correlated with EDSS, SDMT-z and lesion load; disease duration did not relate to myelin content in any of the regions of interest (table 2.8).

Figure 2.8. T1-weighted 3 Tesla images and MyC maps in two MS patients. In A: patient with RRMS, female, 34 years old, disease duration 7 years, EDSS 0, SDMT-z 0.25. In B: patient with SPMS, female, 51 years old, disease duration 29 years, EDSS 7, SDMT-z -2.98. In the SPMS subject, there is remarkable atrophy and the myelin content map (color bar) has lower values.

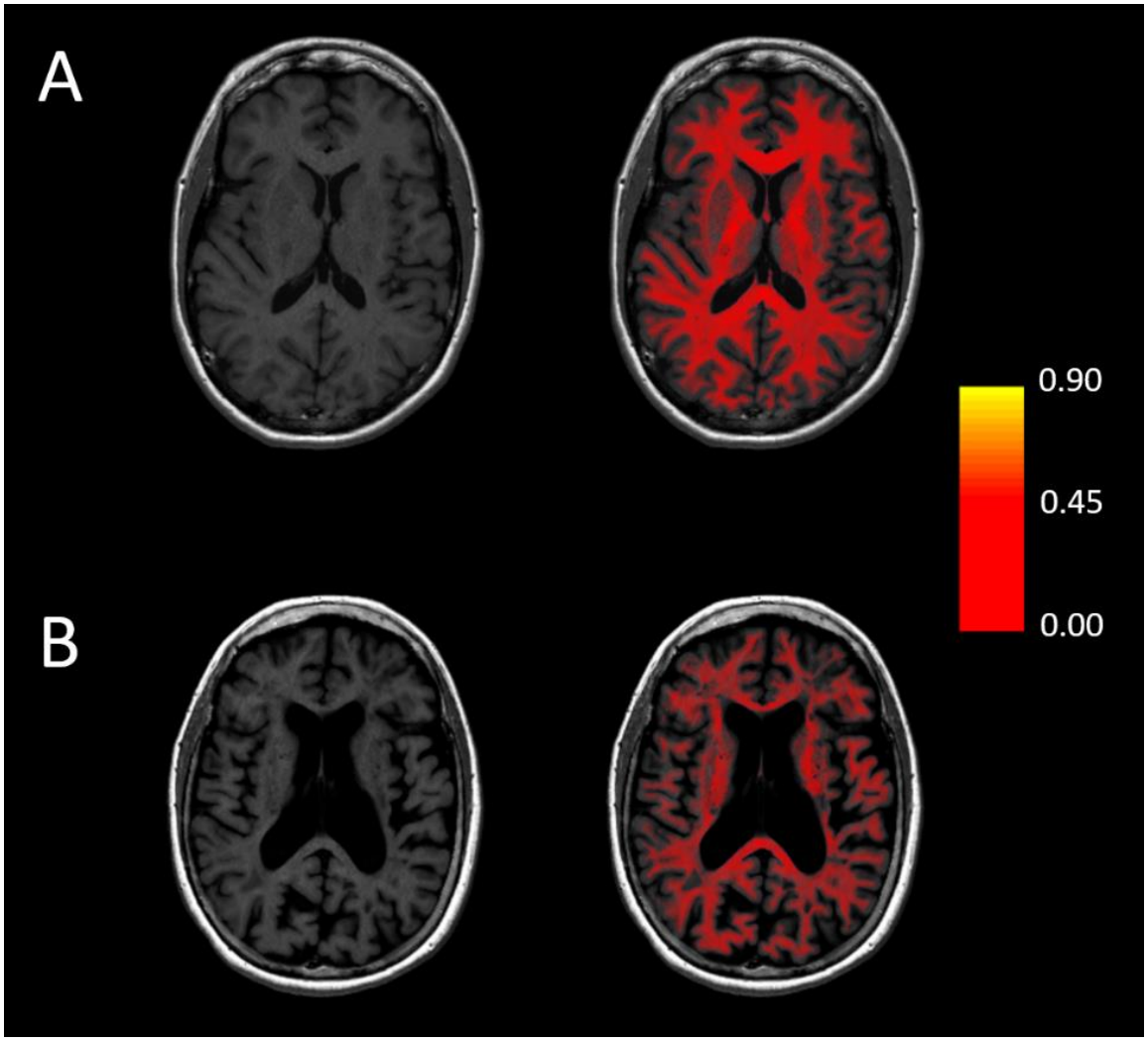

Table 2.7. White matter lesion load and myelin content in the Synthetic MRI patient subgroup.

Radiological characteristic	RRMS	SPMS	*P* value
WML volume mm^3 mean±SD	6156±6626	32496±23193	*0.02**
MyC in NAWM mean±SD	0.27±0.02	0.24±0.03	*0.03**
MyC in WM perilesional areas mean±SD	0.25±0.03	0.22±0.03	*0.09***
MyC in WML mean±SD	0.18±0.03	0.11±0.03	*0.2***

*by Wilcoxon test; **by t test.

Table 2.8. Results from analyses of correlation between myelin content in three regions of interest and clinical metrics. Multilinear regression was performed for EDSS, including age as an adjusting factor. Spearman correlation was applied for SDMT z scores, disease duration and WML volume.

Characteristic	MyC lesion	MyC perilesional	MyC NAWM
EDSS	R^2= 0.36 par. coeff. -16.9 p =0.2	R^2=0.68 par. coeff. -45.6 p =0.0006	R^2 0.77 par. coeff. -54.6 p <0.0001
SDMT-z	Spearman's rho 0.18; p = 0.5	Spearman's rho 0.44; p = 0.07	Spearman's rho 0.57; p = 0.01
disease duration	Spearman's rho -0.31 p = 0.2	Spearman's rho -0.28 p = 0.2	Spearman's rho -34 p = 0.1
WML load	Spearman's rho -0.37 p =0.1	Spearman's rho -0.74 p =0.0004	Spearman's rho -0.84 p <0.0001

2.22 Intra-subject variability of myelin content

The myelin content in the perilesional areas and the NAWM were strongly correlated. A milder correlation was found between WML and perilesional areas, and no correlation between myelin content in lesions and NAWM (figure 2.9).

Values of myelin content were higher in the NAWM and decreased towards the lesions (table 2.9).

Table 2.9. Myelin content in WML, perilesional areas and NAWM in MS patients.

MyC WML mean±SD	0.13±0.03
MyC perilesional mean±SD	0.24±0.03
MyC NAWM mean±SD	0.26±0.03
T test WML vs NAWM	*p value <0.0001*
T test WML vs perilesional	*p value <0.0001*
T test perilesional vs NAWM	*p value <0.0001*

Figure 2.9. Correlation of myelin content values in the WML, perilesional areas and NAWM.

MyC in WML versus perilesional area
Pearson's r = 0.62
p = 0.006
95% CCII 0.22, 0.84

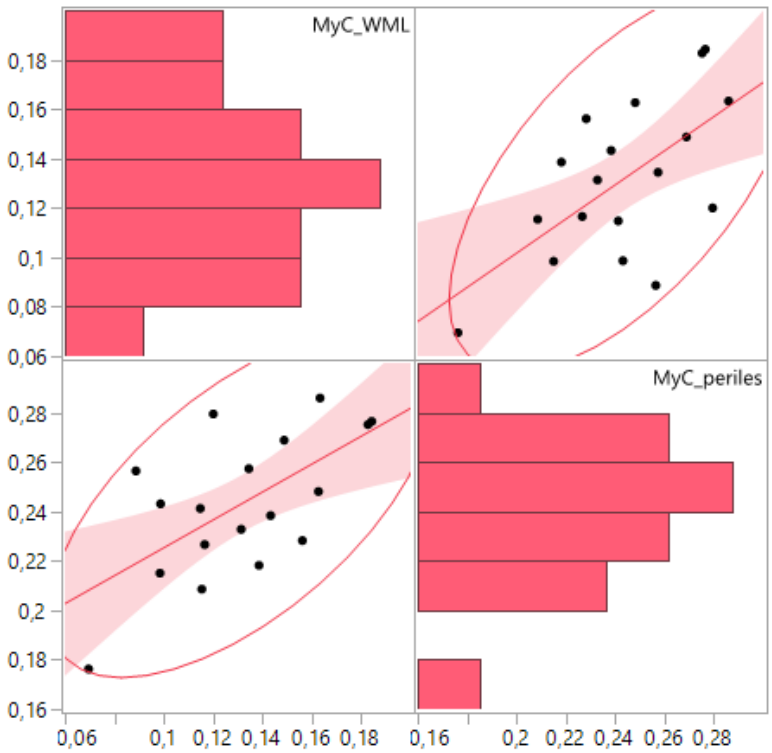

MyC in perilesional areas versus NAWM
Spearman's rho = 0.85
p <0.0001
95% CCII 0.63, 0.94

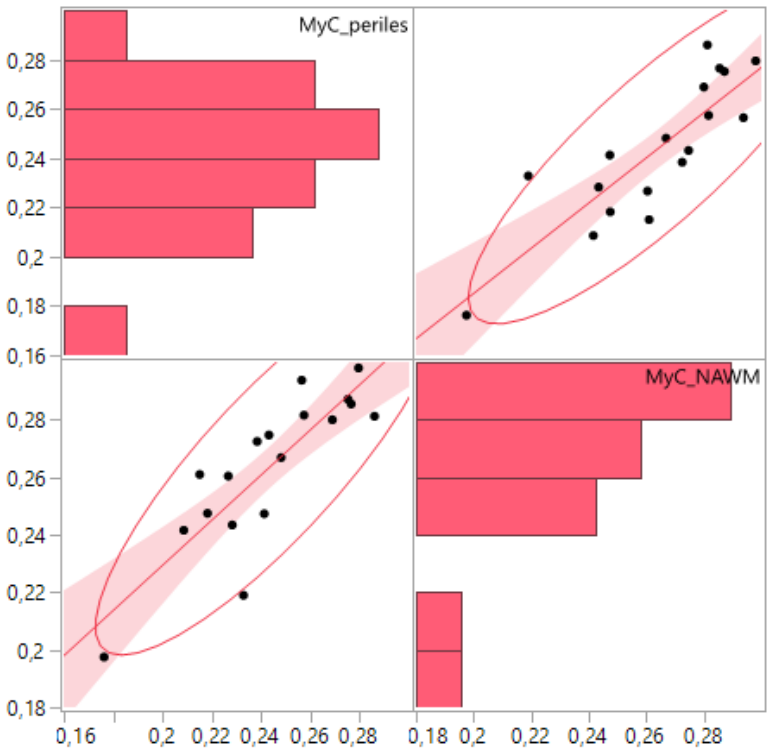

MyC in WML versus NAWM
Spearman's rho = 0.32
p =0.2
95% CCII -0.08, 0.73

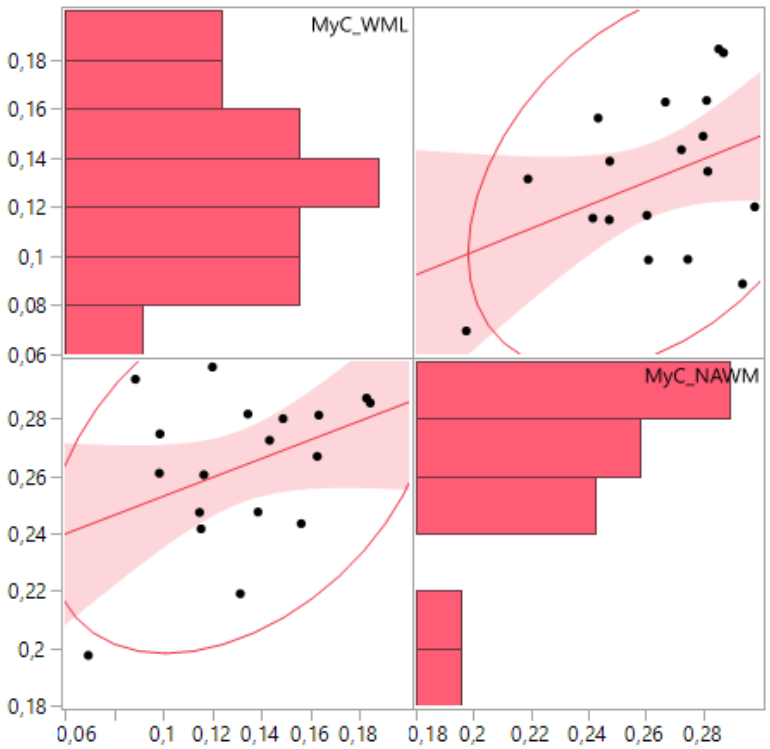

2.23 Correlation of myelin content with ^{11}C-PBR28 uptake

Values of myelin content in NAWM, perilesional areas and WML were related to TSPO uptake in the same regions. A significant correlation or a trend were found for all factors but myelin content in the lesions (table 2.10). The same analysis was repeated for the RRMS group only (table 2.11).

Table 2.10. Spearman's correlation between myelin content and TSPO uptake in white matter lesions, perilesional areas and normal-appearing white matter in all MS subjects.

	MyC WML	MyC perilesional	MyC NAWM
SUVR WML	Spearman's rho -0.15 p =0.5	Spearman's rho -0.69 p =0.001	Spearman's rho -0.64 p = 0.004
SUVR perilesional	Spearman's rho -0.21 p =0.4	Spearman's rho -0.66 p = 0.003	Spearman's rho -0.60 p=0.008
SUVR NAWM	Spearman's rho -0.21 p =0.4	Spearman's rho -0.52 p = 0.03	Spearman's rho -0.43 p=0.08

Table 2.11. Spearman's correlation between myelin content and TSPO uptake in white matter lesions, perilesional areas and normal-appearing white matter in RRMS subjects.

	MyC WML	MyC perilesional	MyC NAWM
SUVR WML	Spearman's rho 0.09 p =0.8	Spearman's rho -0.63 p =0.02	Spearman's rho -0.73 p =0.004
SUVR perilesional	Spearman's rho 0.03 p =0.9	Spearman's rho -0.59 p =0.03	Spearman's rho -0.64 p =0.02
SUVR NAWM	Spearman's rho 0.01 p =1.0	Spearman's rho -0.30 p =0.3	Spearman's rho -0.37 p =0.2

Individual lesion analysis showed that myelin content did not change across different type of lesions (active, inactive, peripherally active), but a difference was seen in the perilesional areas between active and inactive lesions, myelin content being lower in the first type (table 2.12).

Table 2.12. Values of myelin content within white matter lesions and perilesional areas for active, inactive and peripherally active lesions. A matched pairs t test has been performed to compare myelin content in the different lesion types. Lesion and perilesional MyC values are averaged per subject.

	WML	**perilesional areas**
Active lesions MyC mean±SD	0.14±0.06	0.22±0.04
Inactive lesions MyC mean±SD	0.13±0.03	0.25±0.03
Peripherally active lesions MyC mean±SD	0.11±0.09	0.22±0.04
Active vs inactive t test	*p = 0.6*	*p = 0.01*
Active vs peripherally active t test	*p = 0.9*	*p = 0.1*
Peripherally active vs inactive t test	*p = 0.6*	*p = 0.7*

Discussion

In this study, we assessed microglia activation and myelin content in the lesioned and normal-appearing white matter of RRMS and SPMS patients and correlated them to clinical and radiological disease burden.

Microglia activation was abnormally increased in the white matter of MS patients. Although SUVR values were lower in WML than in NAWM, the inflammatory activity in WML correlated the most with disease burden. Patients with high inflammatory activity in the WML showed worse disease outcomes. TSPO uptake showed heterogeneous pattern within lesions. Peripherally active lesions were more common in the progressive disease and related to physical disability. The percentage of active lesions decreased with disease duration, while the percentage of inactive lesions increased.

Myelin content in the NAWM and in the perilesional areas correlated with clinical and radiological metrics. Microglia activation in lesions and non-lesioned white matter inversely correlated with myelin content in the NAWM and perilesional areas.

We performed two different analyses of neuroinflammation. The first measured continuous values of SUVR in three different regions of interest (lesions, perilesional areas, NAWM) and correlated them to myelin content and clinical outcomes.

^{11}C-PBR28 is a second generation radioligand targeting TSPO, whose expression is increased in activated microglia. TSPO expression has been found to be abnormally increased in MS and to correlate with disease severity (Debruyne et al., 2003; Oh et al., 2011; Rissanen et al., 2014; Herranz et al., 2016; Barletta et al., 2020). However, increased TSPO expression is not specific for MS, since it has been detected in other neurological diseases involving neuroinflammation (Alshikho et al., 2018; Albrecht et al., 2019 a/b; Kreisl et al., 2020). Moreover, the interpretation of increased TSPO uptake, in MS and in other diseases, is challenged by some limitations. First, the low cell specificity of TSPO expression, which has also been described in astrocytes in inflammatory environment and in endothelial cells (Lavisse et al., 2012; Rizzo et al., 2017). Second, TSPO expression does not discriminate myeloid derived from the resident microglial cells in the central nervous system and does not distinguish between proinflammatory and protective states of cells (Stankoff et al., 2018).

Microglia activation may play an ambivalent role in the pathogenesis and evolution of MS. It has been proven that, aside its detrimental action, activated microglia can contribute to creating a microenvironment for repair and regenerative processes in demyelinating neuroinflammatory diseases (Napoli and Neumann, 2010; Lombardi et al., 2019). In our study, we found an inverse correlation between microglia activation and myelin content, but this was mostly true for TSPO expression within the lesions. In the NAWM, where tracer uptake had the highest values, the correlation was weaker. It is possible that the protective role of microglia is in effect mostly in the non-lesioned tissue, where both a functional and biological reservoir exist in MS as well as other neurological diseases (Faivre et al., 2016, De Kouchkovsky et al., 2016; Sagnier et al., 2020). This resource for tissue repair and clinical recovery can be targeted by neuroprotective and remyelinating therapies. In this scenario, the discover of more specific markers of neuroinflammation to monitor treatment efficacy becomes crucial. In particular, of greatest importance is the availability of a PET radiotracer that can distinguish between "good" and "bad" microglia, the first being a protective component in the event of a pathological process, the second leading to structural damage and disease progression.

The second type of analysis performed in this study assessed the level of inflammation within the lesions, intended like the inflammatory activity of the WML relative to the NAWM inflammation. Results from this analysis confirmed those of recent *ex vivo* and *in vivo* studies, which focused their attention on the inflammatory state of individual lesions. In these studies, several distinct inflammatory profiles of chronic lesions have been described, with a proportion of WM lesions evolving towards chronic activation and/or a smoldering state, and others becoming inactive. These profiles have been shown to have an impact on disease severity (Frischer et al., 2015; Datta et al., 2017; Absinta et al., 2019). In this direction, TSPO PET has allowed to assess the contribution of chronic active lesions to disability progression in MS. In our study, active lesions, as defined by the presence of higher uptake compared to the surrounding NAWM, showed a reduction as disease duration increased, while inactive lesions showed opposite behaviour. We also found a correlation between peripherally active lesions and EDSS and a predominance of this type of lesions in the progressive disease. Active lesions were found in almost all subjects, including those on highly effective disease modifying therapies. The ongoing inflammation in these subjects can explain why in clinical practice we observe disease progression in absence of clinical relapses.

Despite a reduction of active lesions in the later stages, overall TSPO uptake increased with disease duration proportionally in NAWM and WML, and highly correlated with bad clinical and radiological outcomes. The strong correlation between the NAWM and WML TSPO uptake for individual patients suggests that these measures both reflect the same individually variable, innate inflammatory phenotype (Datta et al., 2017).

The comparison between the two TSPO analyses (the analysis of overall TSPO expression and that of individual lesion inflammation compared to NAWM) points our attention on the biphasic trend of the disease. In the early phase, an increase in brain WML load predicts relapses and subsequently early disability. In this phase, the occurrence of active lesions can be concomitant with the formation of new lesions as detected by conventional MRI. In the second, progressive phase of the disease, when active lesions turn in to inactive or slowly expanding lesions, disability worsening develops independently of WML and relapses, (Fisniku et al., 2008). In this scenario, the disease is considered as "a dual entity, with an adaptative immune-driven inflammatory component linked to WML and relapses, and a diffuse neurodegenerative component responsible for longer term disability accrual" (Stankoff et al., 2018).

Myelin content seems to vary proportionally within each subject in the NAWM and perilesional areas but showed variability in the WML. This may seem obvious, considering the demyelinating nature of MS lesions, but could partially be explained by the limitation of the synthetic MRI technique, that proved to be suboptimal for myelin quantification in lesions. This could also explain why our analysis failed to find correlations between the degree of demyelination in WML and clinical and radiological outcomes, or even a correlation with microglia activation in the lesions.

The strong negative correlation between myelin content in the NAWM and clinical disability suggests the importance of preserving tissue integrity outside the lesioned areas. Therefore, the efficacy of neuroprotective drugs should be assessed especially in the non-lesioned tissue.

A strong inverse correlation was found instead between myelin content in the non-lesioned white matter and SUVR values in all the regions of interest, especially in WML. When considering only the RRMS patients, the correlation between SUVR in WML and myelin content in NAWM increased, but the trend of correlation with SUVR in NAWM was lost.

This could suggest that, at least in the early phase of the disease, microglia activation in the normal-appearing tissue may have a less destructive effect on myelin integrity, while inflammatory activity in the WML is driving towards disability and disease progression.

A difference in myelin content along the perilesional areas was found in active versus non-active lesions. This could be related to the fact that ongoing inflammation obstacles the process of remyelination, although this could still be present in active lesions. Moreover, the newly formed myelin is instable and can be subject to new waves of demyelination (Prineas et al., 1984; Bramow et al., 2010).

The small sample size and the lack of follow-up data for the SyMRI partially limited the potential of this analysis, which needs further investigation on bigger cohorts and longitudinal observation. The lack of a control group for the SyMRI data is another limitation, although the technique has already been validated in MS patients versus healthy controls (Ouellette et al., 2020).

In conclusion, our ^{11}C-PBR28 PET analysis confirmed the new role of this technique in detecting lesion activity for the staging of the disease, which seems to have a prognostic value, with limitations mainly due to the lack of specificity of the radiotracer. On the other hand, the SyMRI proved to be a promising tool for monitoring the efficacy of myelo-protective and remyelinating drugs, but also to assess the protective role of microglia in MS and other neurological disorders.

The combination of the two techniques opens the way to a new approach for the study of the disease pathogenesis, where inflammation and demyelination interact, as well as for assessing the efficacy of new disease modifying treatments.

References

- Absinta M, Sati P, Masuzzo F, Nair G, Sethi V, Kolb H, Ohayon J, Wu T, Cortese ICM, Reich DS. Association of Chronic Active Multiple Sclerosis Lesions With Disability In Vivo. JAMA Neurol. 2019 Dec 1;76(12):1474-1483.
- Albert M, Antel J, Brück W, Stadelmann C. Extensive cortical remyelination in patients with chronic multiple sclerosis. Brain Pathol. 2007 Apr;17(2):129-38.
- Albrecht DS, Mainero C, Ichijo E, Ward N, Granziera C, Zürcher NR, Akeju O, Bonnier G, Price J, Hooker JM, Napadow V, Loggia ML, Hadjikhani N. Imaging of neuroinflammation in migraine with aura: A [11 C]PBR28 PET/MRI study. Neurology. 2019 Apr 23;92(17):e2038-e2050. (a)
- Albrecht DS, Forsberg A, Sandström A, et al. Brain glial activation in fibromyalgia - A multi-site positron emission tomography investigation. Brain Behav Immun. 2019;75:72-83. (b)
- Alshikho MJ, Zürcher NR, Loggia ML, et al. Integrated magnetic resonance imaging and [11 C]-PBR28 positron emission tomographic imaging in amyotrophic lateral sclerosis. Ann Neurol. 2018;83(6):1186-1197.
- Anhoque CF, Neto LB, Aires SC et al. Cognitive impairment in patients with clinically isolated syndrome. Dement Neuropsychol. Oct-Dec 2012;6(4):266-269.
- Badji A, Mangeat G, Ouellette R, Treaba CA, Granberg T, Herranz E. Changes in structural network connectivity in early-stage multiple sclerosis are associated with cortical demyelination. ISMRM. 2016.
- Banati RB, Newcombe J, Gunn RN, Cagnin A, Turkheimer F, Heppner F, Price G, Wegner F, Giovannoni G, Miller DH, Perkin GD, Smith T, Hewson AK, Bydder G, Kreutzberg GW, Jones T, Cuzner ML, Myers R. The peripheral benzodiazepine binding site in the brain in multiple sclerosis: quantitative in vivo imaging of microglia as a measure of disease activity. Brain. 2000 Nov;123 (Pt 11):2321-37.
- Barletta V, Herranz E, Treaba CA, Ouellette R, Mehndiratta A, Loggia ML, Klawiter EC, Ionete C, Jacob SA, Mainero C. Evidence of diffuse cerebellar neuroinflammation in multiple sclerosis by 11C-PBR28 MR-PET. Mult Scler. 2020 May;26(6):668-678.
- Bodini B, Veronese M, García-Lorenzo D, Battaglini M, Poirion E, Chardain A, Freeman L, Louapre C, Tchikviladze M, Papeix C, Dollé F, Zalc B, Lubetzki C,

Bottlaender M, Turkheimer F, Stankoff B. Dynamic Imaging of Individual Remyelination Profiles in Multiple Sclerosis. Ann Neurol. 2016 May;79(5):726-738.

- Braitenberg V. A note on myeloarchitectonics. J Comp Neurol. 1962 Apr;118:141-56.
- Bramow S, Frischer JM, Lassmann H, Koch-Henriksen N, Lucchinetti CF, Sørensen PS, Laursen H. Demyelination versus remyelination in progressive multiple sclerosis. Brain. 2010 Oct;133(10):2983-98.
- Calabrese M, De Stefano N, Atzori M, Bernardi V, Mattisi I, Barachino L, Morra A, Rinaldi L, Romualdi C, Perini P, Battistin L, Gallo. Detection of cortical inflammatory lesions by double inversion recovery magnetic resonance imaging in patients with multiple sclerosis. Arch Neurol. 2007 Oct;64(10):1416-22.
- Calabrese M, Filippi M, Gallo P. Cortical lesions in multiple sclerosis. Nat Rev Neurol. 2010 Aug;6(8):438-44.
- Calabrese M, Rocca MA, Atzori M, Mattisi I, Favaretto A, Perini P, Gallo P, Filippi M. A 3-year magnetic resonance imaging study of cortical lesions in relapse-onset multiple sclerosis. Ann Neurol. 2010b Mar;67(3):376-83.
- Cohen-Adad J, Benner T, Greve D, Kinkel RP, Radding A, Fischl B, Rosen BR, Mainero C. In vivo evidence of disseminated subpial T2* signal changes in multiple sclerosis at 7 T: a surface-based analysis. Neuroimage. 2011 Jul 1;57(1):55-62.
- Cohen-Adad J, Polimeni JR, Helmer KG, Benner T, McNab JA, Wald LL, Rosen BR, Mainero C. T_2* mapping and B_0 orientation-dependence at 7 T reveal cyto- and myeloarchitecture organization of the human cortex. Neuroimage. 2012 Apr 2;60(2):1006-14.
- Collorone S, Cawley N, Grussu F, Prados F, Tona F, Calvi A, Kanber B, Schneider T, Kipp L, Zhang H, Alexander DC, Thompson AJ, Toosy A, Wheeler-Kingshott CAG, Ciccarelli O. Reduced neurite density in the brain and cervical spinal cord in relapsing–remitting multiple sclerosis: A NODDI study. Mult Scler. 2020 Nov;26(13):1647-1657.
- Datta G, Colasanti A, Kalk N, Owen D, Scott G, Rabiner EA, Gunn RG, Lingford-Hughes A, Malik O, Ciccarelli O, Nicholas R, Nei L, Barraglini M, Stefano ND, Matthews PM. 11C-PBR28 and 18F-PBR111 Detect White Matter Inflammatory Heterogeneity in Multiple Sclerosis. J Nucl Med. 2017 Sep;58(9):1477-1482.

- De Kouchkovsky I, Fieremans E, Fleysher L, Herbert J, Grossman RI, Inglese M. Quantification of normal-appearing white matter tract integrityin multiple sclerosis: a diffusion kurtosis imaging study. J Neurol (2016) 263:1146–1155.
- De Santis S, Bastiani M, Droby A, Kolber P, Zipp F, Pracht E, Stoecker T, Groppa S, Roebroeck A. Characterizing Microstructural Tissue Properties in Multiple Sclerosis with Diffusion MRI at 7 T and 3 T: The Impact of the Experimental Design. Neuroscience. 2019 Apr 1;403:17-26.
- Debruyne JC, Versijpt J, Van Laere KJ, De Vos F, Keppens J, Strijckmans K, Achten E, Slegers G, Dierckx RA, Korf J, De Reuck JL. PET visualization of microglia in multiple sclerosis patients using [11C]PK11195. Eur J Neurol 2003; 10: 257–64.
- Derakhshan M, Caramanos Z, Narayanan S, Arnold DL, Louis Collins D. Surface-based analysis reveals regions of reduced cortical magnetization transfer ratio in patients with multiple sclerosis: a proposed method for imaging subpial demyelination. Hum Brain Mapp. 2014 Jul;35(7):3402-13.
- Faivre A, Robinet E, Guye M, Rousseau C, Maarouf A, Le Troter A, Zaaraoui W, Rico A, Crespy L, Soulier E, Confort-Gouny S, Pelletier J, Achard S, Ranjeva J, Audoin B. Depletion of brain functional connectivity enhancement leads to disability progression in multiple sclerosis: A longitudinal resting-state fMRI study. Mult Scler. 2016 Nov;22(13):1695-1708.
- Fan Q, Witzel T, Nummenmaa A, Van Dijk KRA, Van Horn JD, Drews MK, Somerville LH, Sheridan MA, Santillana RM, Snyder J, Hedden T, Shaw EE, Hollinshead MO, Renvall V, Zanzonico R, Keil B, Cauley S, Polimeni JR, Tisdall D, Buckner RL, Wedeen VJ, Wald LL, Toga AW, Rosen BR. MGH-USC Human Connectome Project datasets with ultra-high b-value diffusion MRI. Neuroimage. 2016 Jan 1;124(Pt B):1108-1114.
- Fisniku LK, Brex PA, Altmann DR, Miszkiel KA, Benton CE, Lanyon R, Thompson AJ, Miller DH. Disability and T2 MRI lesions: a 20-year follow-up of patients with relapse onset of multiple sclerosis. Brain. 2008 Mar;131(Pt 3):808-17.
- Frischer JM, Weigand SD, Guo Y, Kale N, Parisi JE, Pirko I, Mandrekar J, Bramow S, Metz I, Brück W, Lassmann H, Lucchinetti CF. Clinical and pathological insights into the dynamic nature of the white matter multiple sclerosis plaque. Ann Neurol. 2015 Nov; 78(5):710–21.

- Fukunaga M, Li TQ, van Gelderen P, de Zwart JA, Shmueli K, Yao B, Lee J, Maric D, Aronova MA, Zhang G, Leapman RD, Schenck JF, Merkle H, Duyn JH. Layer-specific variation of iron content in cerebral cortex as a source of MRI contrast. Proc Natl Acad Sci U S A. 2010 Feb 23;107(8):3834-9.
- Glasser MF, Van Essen DC. Mapping human cortical areas in vivo based on myelin content as revealed by T1- and T2-weighted MRI. J Neurosci. 2011 Aug 10;31(32):11597-616.
- Glasser MF, Coalson TS, Robinson EC, Hacker CD, Harwell J, Yacoub E, Ugurbil K, Andersson J, Beckmann CF, Jenkinson M, Smith SM, Van Essen DC. A multi-modal parcellation of human cerebral cortex. Nature. 2016 Aug 11;536(7615):171-178.
- Goldschmidt T, Antel J, Konig FB, Brück W, Kuhlmann T. Remyelination capacity of the MS brain decreases with disease chronicity. Neurology. 2009 Jun 2;72(22):1914-21.
- Govindarajan ST, Cohen-Adad J, Sormani MP, Fan AP, Louapre C, Mainero C. Reproducibility of T2 * mapping in the human cerebral cortex in vivo at 7 tesla MRI. J Magn Reson Imaging. 2015 Aug;42(2):290-6.
- Granberg T, Fan Q, Treaba CA, Ouellette R, Herranz E, Mangeat G, Louapre C, Cohen-Adad J, Klawiter EC, Sloane JA, Mainero C. In vivo characterization of cortical and white matter neuroaxonal pathology in early multiple sclerosis. Brain. 2017 Nov; 140(11): 2912–2926.
- Greve DN, Fischl B. Accurate and robust brain image alignment using boundary-based registration. Neuroimage. 2009 Oct 15;48(1):63-72.
- Grussu F, Schneider T, Tur C, Yates RL, Tachrount M, Ianus A, Yiannakas MC, Newcombe J, Zhang H, Alexander DC, DeLuca GC, Wheeler-Kingshott CAG. Neurite dispersion: a new marker of multiple sclerosis spinal cord pathology? Ann Clin Transl Neurol. 2017 Aug 15;4(9):663-679.
- Guglielmetti C, Veraart J, Roelant E, Mai Z, Daans J, Van Audekerke J, Naeyaert M, Vanhoutte G, Delgado Y Palacios R, Praet J, Fieremans E, Ponsaerts P, Sijbers J, Van der Linden A, Verhoye M. Diffusion kurtosis imaging probes cortical alterations and white matter pathology following cuprizone induced demyelination and spontaneous remyelination. Neuroimage. 2016 Jan 15;125:363-377.
- Haacke EM, Makki M, Ge Y, Maheshwari M, Sehgal V, Hu J, Selvan M, Wu Z, Latif Z, Xuan Y, Khan O, Garbern J, Grossman RI. Characterizing iron deposition in

multiple sclerosis lesions using susceptibility weighted imaging. J Magn Reson Imaging. 2009 Mar; 29(3): 537–544.

- Herranz E, Giannì C, Louapre C, Treaba CA, Govindarajan St, Ouellette R, Loggia ML, Sloane JA, Madigan N, Izquierdo-Garcia D, Ward N, Mangeat G, Granberg T, Klawiter EC, Catana C, Hooker JM, Taylor N, Ionete C, Kinkel RP, Mainero C. Neuroinflammatory component of gray matter pathology in multiple sclerosis. Ann Neurol. 2016 Nov;80(5):776-790.
- Herranz E, Louapre C, Treaba CA, Govindarajan ST, Ouellette R, Mangeat G, Loggia ML, Cohen-Adad J, Klawiter EC, Sloan JA, Mainero C. Profiles of cortical inflammation in multiple sclerosis by 11C-PBR28 MR-PET and 7 Tesla imaging. Mult Scler. 2020 Oct;26(12):1497-1509.
- Jespersen SN, Bjarkam CR, Nyengaard JR, Chakravarty MM, Hansen B, Vosegaard T, Østergaard L, Yablonskiy D, Nielsen NC, Vestergaard-Poulsen P. Neurite density from magnetic resonance diffusion measurements at ultrahigh field: comparison with light microscopy and electron microscopy. Neuroimage. 2010 Jan 1;49(1):205-16.
- Kilsdonk ID, Jonkman LE, Klaver R, van Veluw SJ, Zwanenburg JJ, Kuijer JP, Pouwels PJ, Twisk JW, Wattjes MP, Luijten PR, Barkhof F, Geurts JJ. Increased cortical grey matter lesion detection in multiple sclerosis with 7 T MRI: a post-mortem verification study. Brain. 2016 May;139(Pt 5):1472-81.
- Koenig SH, Brown RD 3rd, Spiller M, Lundbom N. Relaxometry of brain: why white matter appears bright in MRI. Magn Reson Med. 1990 Jun;14(3):482-95.
- Kolb A, Wehrl HF, Hofmann M, Judenhofer MS, Eriksson L, Ladebeck R, Lichy MP, Byars L, Michel C, Schlemmer H, Schmand M, Claussen CD, Sossi V, Pichler BJ. Technical performance evaluation of a human brain PET/MRI system. Eur Radiol 2012; 22(8): 1776–1788.
- Kreisl WC, Kim M, Coughlin JM, Henter ID, Owen DR, Innis RB. PET imaging of neuroinflammation in neurological disorders. Lancet Neurol. 2020 Nov;19(11):940-950.
- Kuhlmann T, Ludwin S, Prat A, Antel J, Brück W, Lassmann H. An updated histological classification system for multiple sclerosis lesions. Acta Neuropathol. 2017 Jan;133(1):13-24.

- Kutzelnigg A, Lucchinetti CF, Stadelmann C, Brück W, Rauschka H, Bergmann M, Schmidbauer M, Parisi JE, Lassmann H. Cortical demyelination and diffuse white matter injury in multiple sclerosis. Brain. 2005 Nov;128(Pt 11):2705-12.
- Lassmann H. The Pathologic Substrate of Magnetic Resonance Alterations in Multiple Sclerosis. Neuroimaging Clin N Am. 2008 Nov;18(4):563-76, ix.
- Lassmann H, Bradl M. Multiple sclerosis: experimental models and reality. Acta Neuropathol. 2017 Feb;133(2):223-244.
- Lavisse S, Guillermier M, Herard A-S, Petit F, Delahaye M, Van Camp N, Ben Haim L, Lebon V, Remy P, Dollé F, Delzescaux T, Bonvento G, Hantraye P, Escartin C. Reactive astrocytes overexpress TSPO and are detected by TSPO positron emission tomography imaging. J Neurosci. 2012 Aug 8;32(32):10809-18.
- Lee NJ, Ha SK, Sati P, Absinta M, Nair G, Luciano NJ, Leibovitch EC, Yen CC, Rouault TA, Silva AC, Jacobson S, Reich DS. Potential role of iron in repair of inflammatory demyelinating lesions. J Clin Invest. 2019 Oct 1;129(10):4365-4376.
- Lombardi M, Parolisi R, Scaroni F, Bonfanti E, Gualerzi A, Gabrielli M, Kerlero de Rosbo N, Uccelli A, Giussani P, Viani P, Garlanda C, Abbracchio MP, Chaabane L, Buffo A, Fumagalli M, Verderio C. Detrimental and protective action of microglial extracellular vesicles on myelin lesions: astrocyte involvement in remyelination failure. Acta Neuropathol. 2019 Dec;138(6):987-1012.
- Louapre C, Govindarajan ST, Giannì C, Langkammer C, Sloane JA, Kinkel RP, Mainero C. Beyond focal cortical lesions in MS: An in vivo quantitative and spatial imaging study at 7T. Neurology. 2015 Nov 10; 85(19): 1702–1709.
- Lucchinetti C, Brück W, Parisi J, Scheithauer B, Rodriguez M, Lassmann H (2000) Heterogeneity of multiple sclerosis lesions: implications for the pathogenesis of demyelination. Ann Neurol. 2000 Jun;47(6):707-17.
- Lucchinetti CF, Popescu BF, Bunyan RF, Moll NM, Roemer SF, Lassmann H, Brück W, Parisi JE, Scheithauer BW, Giannini C, Weigand SD, Mandrekar J, Ransohoff RM. Inflammatory cortical demyelination in early multiple sclerosis. N Engl J Med. 2011 Dec 8;365(23):2188-97.
- Ludwin SK. The neuropathology of multiple sclerosis. Neuroimaging Clin N Am. 2000 Nov;10(4):625-48 ,vii.

- Mainero C, Louapre C, Govindarajan ST, Giannì C, Nielsen AS, Cohen-Adad J, Sloane J, Kinkel RP. A gradient in cortical pathology in multiple sclerosis by in vivo quantitative 7 T imaging. Brain. 2015 Apr;138(Pt 4):932-45.
- Mangeat G, Govindarajan ST, Mainero C, Cohen-Adad J. Multivariate combination of magnetization transfer, T2* and B0 orientation to study the myelo-architecture of the in vivo human cortex. Neuroimage. 2015 Oct 1;119:89-102.
- Mangeat G, Govindarajan ST, Kinkel RP, Mainero C, Cohen-Adad J. Multivariate combination of magnetization transfer ratio and quantitative T, to detect subpial demyelination in multiple sclerosis. ISMRM. 2015b.
- Mangeat G, Ouellette R, Treaba CA, Granberg T, Herranz E, Louapre C, … Cohen-Adad J. Association between cortical demyelination and structural connectomics in early multiple sclerosis. ISMRM. 2016.
- Mangeat G, Badji A, Ouellette R, Treaba CA, Herranz E, Granberg T, Louapre C, Stikov N, Sloane JA, Bellec P, Mainero C, Cohen-Adad J. Changes in structural network are associated with cortical demyelination in early multiple sclerosis. Hum Brain Mapp. 2018 May; 39(5): 2133–2146.
- Menascu S, Stern M, Aloni R et al. Assessing cognitive performance in radiologically isolated syndrome. Mult Scler Relat Disord. 2019 Jul;32:70-73.
- Nakamura K, Chen JT, Ontaneda D, Fox RJ, Trapp BD. T1-/T2-weighted ratio differs in demyelinated cortex in multiple sclerosis. Ann Neurol. 2017 Oct;82(4):635-639.
- Napoli I, Neumann H. Protective effects of microglia in multiple sclerosis. Exp Neurol. 2010 Sep;225(1):24-8.
- Oh U, Fujita M, Ikonomidou VN, Evangelou IE, Matsuura E, Harberts E, Fujimura Y, Richert ND, Ohayon J, Pike VW, Zhang Y, Zoghbi SS, Innis RB, Jacobson S. Translocator protein PET imaging for glial activation in multiple sclerosis. J Neuroimmune Pharmacol 2011; 6: 354–61.
- Orthmann-Murphy J, Call CL, Molina-Castro GC et al. Remyelination alters the pattern of myelin in the cerebral cortex. Elife. 2020 May 27;9:e56621.
- Ouellette R, Mangeat G, Polyak I, Warntjes M, Forslin Y, Bergendal Å, Plattén M, Uppman M, Treaba CA, Cohen-Adad J, Piehl F, Kristoffersen Wiberg Maria, Fredrikson S, Mainero C, Granberg T. Validation of Rapid Magnetic Resonance Myelin Imaging in Multiple Sclerosis. Ann Neurol. 2020 May;87(5):710-724.

- Owen DR, Yeo AJ, Gunn RN, Song K, Wadsworth G, Lewis A, Rhodes C, Pulford DJ, Bennacef I, Parker CA, St Jean PL, Cardon LR, Mooser VE, Matthews PM, Rabiner EA, Rubio JP. An 18-kDa translocator protein (TSPO) polymorphism explains differences in binding affinity of the PET radioligand PBR28. J Cereb Blood Flow Metab. 2012 Jan;32(1):15.
- Parmenter BA, Testa SM, Schretlen DJ, Weinstock-Guttman B, Benedict RH. The utility of regression-based norms in interpreting the minimal assessment of cognitive function in multiple sclerosis (MACFIMS). J Int Neuropsychol Soc. 2010 Jan;16(1):6-16.
- Patrikios P, Stadelmann C, Kutzelnigg A, Rauschka H, Schmidbauer M, Laursen H, Sorensen PS, Brück W, Lucchinetti C, Lassmann H. Remyelination is extensive in a subset of multiple sclerosis patients. Brain. 2006 Dec;129(Pt 12):3165-72.
- Pawlitzki M, Neumann J, Kaufmann J et al. Loss of corticospinal tract integrity in early MS disease stages. Neurol Neuroimmunol Neuroinflamm. 2017 Sep 25;4(6):e399.
- Peterson JW, Bö L, Mörk S, Chang A, Trapp BD. Transected neurites, apoptotic neurons, and reduced inflammation in cortical multiple sclerosis lesions. Ann Neurol. 2001 Sep;50(3):389-400.
- Pitt D, Boster A, Pei W, Wohleb E, Jasne A, Zachariah CR, Rammohan K, Knopp MV, Schmalbrock P. Imaging cortical lesions in multiple sclerosis with ultra-high-field magnetic resonance imaging. Arch Neurol. 2010 Jul;67(7):812-8.
- Polman CH, Reingold SC, Banwell B, Clanet M, Cohen JA, Filippi M, Fujihara K, Havrdova E, Hutchinson M, Kappos L, Lublin FD, Montalban X, O'Connor P, Sandberg-Wollheim M, Thompson AJ, Waubant E, Weinshenker B, Wolinsky JS. Diagnostic criteria for multiple sclerosis: 2010 revisions to the McDonald criteria. Ann Neurol. 2011 Feb;69(2):292-302.
- Prineas JW, Kwon EE, Cho ES, Sharer LR. Continual breakdown and regeneration of myelin in progressive multiple sclerosis plaques. Ann N Y Acad Sci. 1984;436:11-32.
- Righart R, Biberacher V, Jonkman LE, Klaver R, Schmidt P, Buck D, Berthele A, Kirschke JS, Zimmer C, Hemmer B, Geurts JJG, Mühlau M. Cortical pathology in multiple sclerosis detected by the T1/T2-weighted ratio from routine magnetic resonance imaging. Ann Neurol. 2017 Oct;82(4):519-529.

- Rissanen E, Tuisku J, Rokka J, Paavilainen T, Parkkola R, Rinne JO, Airas L. In vivo detection of diffuse inflammation in secondary progressive multiple sclerosis using PET imaging and the radioligand 11C-PK11195. J Nucl Med 2014;55: 939–44.
- Rizzo G, Veronese M, Tonietto M, Bodini B, Stankoff B, Wimberley C, Lavisse S, Bottlaender M, Bloomfield PS, Howes O, Zanotti-Fregonara P, Turkheimer FE, Bertoldo A. Generalization of endothelial modelling of TSPO PET imaging: considerations on tracer affinities. J Cereb Blood Flow Metab. 2019 May;39(5):874-885.
- Sagnier S, Catheline G, Dilharreguy B, Linck P, Coupé P, Munsch F, Bigourdan A, Debruxelles S, Poli M, Olindo S, Renou P, Rouanet F, Dousset V, Berthoz S, Tourdias T, Sibon I. Normal-Appearing White Matter Integrity Is a Predictor of Outcome After Ischemic Stroke. Stroke. 2020 Feb;51(2):449-456.
- Schmierer K, Parkes HG, So PW, An SF, Brandner S, Ordidge RJ, Yousry TA, Miller DH. High field (9.4 Tesla) magnetic resonance imaging of cortical grey matter lesions in multiple sclerosis. Brain. 2010 Mar;133(Pt 3):858-67.
- Schneider T, Brownlee W, Zhang H, Ciccarelli O, Miller DH, Wheeler-Kingshott CG. Sensitivity of multi-shell NODDI to multiple sclerosis white matter changes: a pilot study. Funct Neurol. 2017;32(2):97-101.
- Seti V, Nair G, Absinta M, Sati P, Venkataraman A, Ohayon J, Wu T, Yang K, Shea C, Dewey BE, Cortese IR, Reich DS. Slowly Eroding Lesions in Multiple Sclerosis. Mult Scler. 2017 Mar;23(3):464-472.
- Stankoff B, Poirion E, Tonietto M, Bodini B. Exploring the heterogeneity of MS lesions using positron emission tomography: a reappraisal of their contribution to disability. Brain Pathol. 2018 Sep;28(5):723-734.
- Strijbis EMM1, Kooi EJ1, van der Valk P1, Geurts JJG1. Cortical Remyelination Is Heterogeneous in Multiple Sclerosis. J Neuropathol Exp Neurol. 2017 May 1;76(5):390-401.
- Stüber C, Morawski M, Schäfer A, Labadie C, Wähnert M, Leuze C, Streicher M, Barapatre N, Reimann K, Geyer S, Spemann D, Turner R. Myelin and iron concentration in the human brain: a quantitative study of MRI contrast. Neuroimage. 2014 Jun;93 Pt 1:95-106.
- Treaba CA, Granberg TE, Sormani MP, Herranz E, Ouellette RA, Louapre C, Sloane JA, Kinkel RP, Mainero C. Longitudinal Characterization of Cortical Lesion

Development and Evolution in Multiple Sclerosis with 7.0-T MRI. Radiology. 2019 Jun;291(3):740-749.

- Turken A, Whitfield-Gabrieli S, Bammer R et al. Cognitive processing speed and the structure of white matter pathways: convergent evidence from normal variation and lesion studies. Neuroimage. 2008 Aug 15;42(2):1032-44.
- Van der Kouwe AJW, Benner T, Salat DH, Fischl B. Brain morphometry with multiecho MPRAGE. Neuroimage. 2008 Apr 1;40(2):559-569.
- Van der Star BJ, Vogel DY, Kipp M, Puentes F, Baker D, Amor S. In vitro and in vivo models of multiple sclerosis. CNS Neurol Disord Drug Targets. 2012 Aug;11(5):570-88.
- Van der Valk P, De Groot CJA. Staging of multiple sclerosis (MS) lesions: pathology of the time frame of MS. Neuropathol Appl Neurobiol. 2000 Feb;26(1):2-10.
- Warntjes M, Engström M, Tisell A, Lundberg P. Modelling the presence of myelin and oedema in the brain based on multi-parametric quantitative MRI. Front Neurol. 2016 Feb 17;7:16.
- Zhang H, Schneider T, Wheeler-Kingshott CAG, Alexander DC. NODDI: Practical in vivo neurite orientation dispersion and density imaging of the human brain. Neuroimage. 2012 Jul 16;61(4):1000-16.